

A Global Optimization Scheme for Bimetallic Nanoparticles



Keisuke Takahashi

Department of Materials and Manufacturing Technology

Department of Applied Physics

Chalmers University of Technology

Thesis submitted for the degree of

Master of Science

June 2011

A Global Optimization Scheme for Bimetallic Nanoparticles

© Keisuke Takahashi, 2011

Examiner: Henrik Grönbeck

Department of Applied Physics

Chalmers University of Technology, 41296 Göteborg, Sweden

Day of thesis defense: June 15th, 2011

I would like to dedicate to my parents, Masakatsu Takahashi and Mieko Takahashi, and my grandfather Shigeru Saito, all of whom have constantly supported me and guided me throughout my studies both at home and abroad.

Acknowledgements

I would like to thank Henrik Grönbeck for not only giving me the chance to complete this project, but also for his continual guidance throughout the span of the project.

I would also like to thank Anders Hellman, for his assistance during the development phase of the program and for his overall assistance with the programming aspect of the project;

Jakub Baran, for teaching me about Density Functional Theory;

Lauro Oliver Paz Borbon, for his assistance with Basin-Hopping and cluster structures;

and Lauren Akif for graphical assistance and for her support and encouragement during the project.

Abstract

The nature of atomic clusters has increasingly attracted the attention of researchers over the last few decades. One of the primary reasons for the rise in interest is that the physical and chemical properties of atomic metal clusters are different from their corresponding bulk metals. To understand cluster properties, knowledge of the relevant structures are needed. However, structural information is very difficult to acquire from experiments. In this thesis, a theoretical approach is used instead. In particular, a Basin-Hopping global optimization algorithm is implemented where the atomic interactions are calculated from first principles by use of the Density Functional Theory (DFT). The Basin-Hopping code is written with the Python programming language and the Siesta and Dmol softwares are used to run the DFT calculations. Structures of bimetallic structures are the primary focus, as they are known as highly-effective hydrogenation catalysts. In addition, the monometallic cluster structures of Sn and Ru are explored. Sn clusters in a range from 2 to 20 atoms with higher stability than previously reported structures were obtained. The optimized Ru clusters match with previous reported results. The electronic, magnetic, and chemical properties of ground state clusters are discussed. The new method was, furthermore, used to study structures of a range of bimetallic systems including Ru-Sn, Ru-Pd, Pd-Au, and other similar structures.

Keywords: Basin-Hopping, Density Functional Theory, Atomic Clusters, Ruthenium, Tin

Contents

Contents	iv
List of Figures	viii
1 Introduction	1
1.1 Overview of Atomic Clusters	1
1.2 Structure	3
1.3 Experimental Methods	4
1.3.1 Cluster Synthesis	4
1.3.2 Characterization	5
1.4 Metal Clusters	8
1.4.1 Ruthenium	8
1.4.2 Tin	8
1.4.3 Ruthenium Tin	8
1.5 Applications	8
1.5.1 Catalysis	8
1.5.2 Magnetic Applications	9
1.5.3 Hydrogen Storage	9
1.5.4 Biodiagnostics	10
2 Theoretical Background	11
2.1 Potential Energy Surface (PES)	11
2.2 Lennard-Jones Potential	11
2.3 Density Functional Theory	13
2.4 Cluster Relaxation	14

CONTENTS

2.5	Energetic Analysis	14
2.5.1	Atomic Unit	14
2.5.2	Binding Energy	14
2.5.3	Vertical Electron Affinity	16
2.6	Distance Analysis	16
2.7	Electronic and Magnetic Properties Analysis	16
3	Global Optimization Schemes	18
3.1	Genetic Algorithm	18
3.2	Basin-Hopping Algorithm	19
3.2.1	Overview	19
3.2.2	Monte Carlo Method	19
3.2.3	Metropolis-Hastings Algorithm	20
3.2.4	Methodology	20
4	Methodology	24
4.1	Tools	24
4.1.1	Atomic Simulation Environment	24
4.1.2	Avogadro	25
4.1.3	Density-Functional Theory Softwares	25
4.1.4	Supercomputer	25
4.2	Simulation with ASE	25
4.2.1	Simulating Lennard-Jones Clusters	25
4.2.2	Construct Random Initial Structure for Monometallic Clusters	26
4.3	Basin-Hopping Code	27
4.3.1	User Input	27
4.3.2	Energy Function	27
4.3.3	Move Strategies Function	27
4.3.4	Run Function	28
4.3.5	Flow Chart for Basin-Hopping Code	28
4.4	Test with Lennard-Jones Potential	30
4.4.1	Single Lennard-Jones Clusters	30

CONTENTS

4.4.2	Binary Lennard-Jones Clusters	30
4.5	Evaluations Tools	33
4.5.1	Read Energy Code	33
4.5.2	Histograms Code	35
4.5.3	Bar Chart Code	35
4.5.4	Read Different Structural Coordinate Extension Code	35
4.5.5	Sort the Local Minimum Structures by Order of Energy Code	35
4.5.6	Re-relaxation Code	36
4.5.7	Measure Distance Code	36
4.6	Move Strategies Analysis	36
4.7	Relaxation Method Test	39
4.8	BH Implementation in SIESTA	39
4.9	Implementation of Dmol	42
5	Sn Clusters	44
5.1	Basin-Hopping Sn Clusters	44
5.2	Relax the Selected Structures from Basin-Hopping Results	46
5.3	Structural Analysis	47
5.4	Energetic Analysis	51
5.4.1	Binding Energy	51
5.4.2	HOMO-LUMO Gap	53
5.4.3	Negatively Charged Sn Clusters	53
6	Ru Clusters	57
6.1	Basin-Hopping Ru Clusters	57
6.2	Relax the Selected Structures from Basin-Hopping Results	58
6.3	Energetic Analysis	60
6.3.1	Binding Energy	60
6.3.2	HOMO-LUMO Gap and Magnetic Properties	60
7	Ru-Sn Clusters	63
7.1	Basin-Hopping, Ru-Sn	63
7.2	Relax the Selected Structures from Basin-Hopping Results	64
7.3	Structure Analysis	64

CONTENTS

7.4	Energetic Analysis	64
7.4.1	Binding Energy	64
7.4.2	HOMO-LUMO Gap	66
7.5	Ru-Sn Clusters Supported on SiO ₂	67
8	Basin-Hopping with Hydrogen Atom	70
8.1	Sn Clusters with Hydrogen	70
8.2	Ru Clusters with Hydrogen	72
8.3	Ru-Sn Clusters with Hydrogen	72
8.4	Binding Energy of Hydrogen	72
9	Conclusions	76
	Appendix A: Structures of Monometallic Clusters	78
	Appendix B: Structures of Bimetallic Clusters	84
	References	94

List of Figures

1.1	Schematic representation of how a certain property may evolve as a function of cluster size.	2
1.2	(a) Li_4 Planar (b) Li_4 3D	4
2.1	The Lennard Jones Potential.	12
3.1	Example of a Basin-Hopping step.	22
3.2	Basin-Hopping energy landscape.	23
4.1	Schemes for the Basin-Hopping method.	29
4.2	Structures for Lennard-Jones clusters obtained with the Basin-Hopping method.	31
4.3	Structures for Binary Lennard-Jones clusters obtained with the Basin-Hopping method.	34
4.4	Histograms for number of found global minima	38
4.5	Optimized Na_8 clusters, where structure 1 corresponds to the global minima.	41
5.1	Ground States Structures for Sn_1 - Sn_{10} clusters.	48
5.2	Ground States Structures for Sn_{11} - Sn_{20} clusters.	49
5.3	Mean distances of Sn clusters.	51
5.4	Binding energy of small Sn clusters.	52
5.5	HOMO-LUMO gap of Sn clusters of 1-20 atoms.	54
5.6	Structures of anionic Sn clusters which are found to have different structures compared to neutral ones.	55

LIST OF FIGURES

5.7	Comparison of experimental and theoretical vertical electron affinity of Sn clusters. Experimental values are taken from [32].	56
6.1	Ground States Structures for Ru ₁ - Ru ₁₂ clusters.	59
6.2	Binding energy for Ru clusters.	61
6.3	HOMO-LUMO gap of Ru clusters of 1-20 atoms.	61
7.1	Ground state structures of Ru _X Sn _Y , X+Y≤16.	65
7.2	Mean distance in Ru-Sn clusters.	66
7.3	HOMO-LUMO gap for Ru-Sn clusters.	67
7.4	Ground States structures of Ru ₁ Sn ₁ ,Ru ₂ Sn ₂ on SiO ₂ surface. . . .	68
7.5	Ground States structures of Ru ₃ Sn ₃ ,Ru ₄ Sn ₄ on SiO ₂ surface. . . .	69
7.6	Ground States structures of Ru ₅ Sn ₅ ,Ru ₆ Sn ₆ on SiO ₂ surface. . . .	69
8.1	Ground state Sn clusters(1-6 atoms) with 1 chemisorption hydrogen atom.	71
8.2	Ground state Ru clusters(1-6 atoms) with 1 chemisorption hydrogen atom.	73
8.3	Ground state Ru-Sn clusters(1-6 atoms) with 1 chemisorption hydrogen atom.	74
8.4	Binding energy of an hydrogen atom in each system.	75
1	Ground States Structures for Au ₁ - Au ₁₀	79
2	Ground States Structures for Ag ₁ - Ag ₉	80
3	Ground States Structures for Cu ₁ - Cu ₈	81
4	Ground States Structures for Pt ₁ - Pt ₁₀	82
5	Ground States Structures for Pd ₁ - Pd ₁₀	83
6	Ground States structures of Ni _X Pd _Y , X+Y≤12.	85
7	Ground States structures of Pd _X Au _Y , X+Y≤12.	86
8	Ground States structures of Pt _X Sn _Y , X+Y≤12.	87
9	Ground States structures of Ru _X Au _Y , X+Y≤12.	88
10	Ground States structures of Ru _X Ag _Y , X+Y≤12.	89
11	Ground States structures of Ru _X Cu _Y , X+Y≤12.	90
12	Ground States structures of Ru _X Ge _Y , X+Y≤12.	91

LIST OF FIGURES

13	Ground States structures of Ru_XPd_Y , $X+Y \leq 12$	92
14	Ground States structures of Ru_XPt_Y , $X+Y \leq 12$	93

Chapter 1

Introduction

1.1 Overview of Atomic Clusters

Theoretical and experimental studies of atomic metal clusters has grown into an important research area during the past few decades. One of the motivations for this research is the novel properties of atomic metal clusters. Physical and chemical properties are generally in clear variance with respect to the corresponding bulk metals.

The first experiment for cluster studies was performed with mass spectrometer ion sources in 1956 by E.W. Becker [1]. In 1960, clusters were produced through the evaporation of metal, releasing the particles into the air to be contained and rendered able to study through a molecular beam. By the 1980s, most of the elements on the periodic table could be produced as atomic clusters through the development of laser vaporization techniques. However, there is still no direct way to determine the structure of the atomic cluster. In the 1990s, researchers shifted their approach to theoretical studies. The development of global optimization algorithms, such as Basin-Hopping, and first-principle methodologies, such as Density Functional Theory, along with the rise in supercomputer power made it possible to explore the structures of the atomic clusters of up to a few hundred atoms.

In physics and chemistry, atomic clusters are defined as an aggregate of atoms. However, terms such as molecules and nanoparticles are also aggregates of atoms.

Molecules such as H_2O , N_2 , and H_2 form an aggregate of atoms in nature. Those molecules exist in an ambient environment. However, atomic clusters are synthesized in a laboratory environment and, in most cases, are only stable in a vacuum or inert environments. Interactions between atoms in atomic clusters are generally stronger than the interaction between closed-shell molecules; however, this is dependent on the cluster elements, as noble gas clusters have weak interactions. Because of this, atomic clusters are able to form larger clusters. The size, composition, and atomic structures of molecules are fixed by a natural limit, while atomic clusters are characterized by size, composition, and even structures and, therefore, are not bound by natural limitations. Thus it can be concluded that the stabilities of atomic clusters are strongly dependent on their sizes, compositions, and structure.

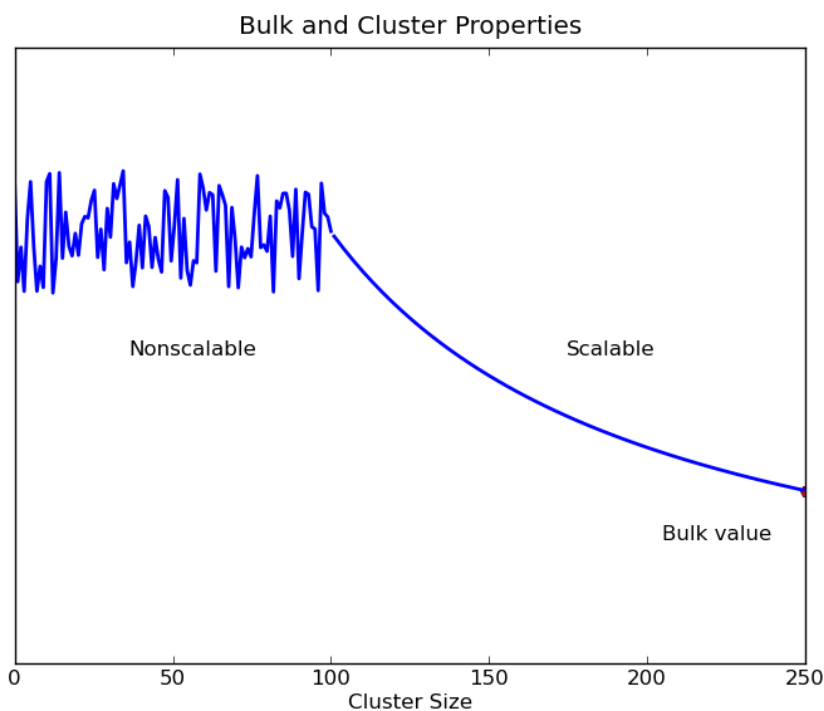


Figure 1.1: Schematic representation of how a certain property may evolve as a function of cluster size.

The difference between atomic clusters and nanoparticles is more difficult

to determine. Figure 1.1 illustrates that intrinsic properties of clusters are size dependent and non-scalable. However, these properties become scalable, at which point the cluster can then be defined as a nanoparticle. In this case, the properties can be scaled from the corresponding bulk properties.

The size and composition can completely determine the properties for atomic clusters. Therefore, the evolution of the atomic clusters eventually leads the clusters to nanoparticles. It must be noted here that the evolution of nanoparticles with their properties are approximately following smooth curve while properties of atomic clusters are not.

However, in most cases atomic clusters have completely different structure than their bulk states. Structures of small gold clusters are particularly interesting. Their ground states structures are planar up to size 12. However, they start to form three-dimensional structures after size 12 and eventually form face centered cubic (fcc) structures. The main difference between cluster and bulk structures is the surface to volume ratio. The surface to volume ratio decreases with increasing the cluster size. When clusters are small and their surface-to-volume ratio is high, they have more surface atoms than atoms with full bulk coordination. Therefore, surface properties of elements are an important factor. Similarly, gold as a bulk material is inert. However, gold clusters are very reactive, making them very important in the catalysis field [2]. Moreover, non-magnetic materials could be magnetic when reducing their sizes. Conductive metal can be insulators. Opaque materials could be transparent. There are many possibilities of tailoring new materials by knowing cluster properties. This fact opens up new fields not only in material science, but also in physics, biology, and chemistry, with the possibility of technological applications in diverse areas such as heterogeneous catalysis and environmental chemistry, among others.

1.2 Structure

Knowing the structures of atomic clusters up to a few hundred atoms is one of the fundamental questions of the field, as the structures will determine the corresponding chemical and physical properties. One example is Li_4 , which has several isomers that exhibit different properties.

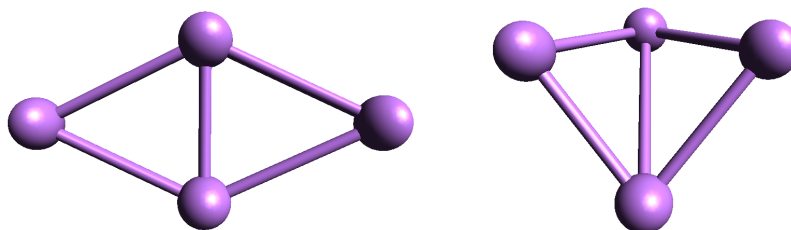


Figure 1.2: (a) Li_4 Planar (b) Li_4 3D

obtained

Li_4 has several different structures, two of which can be seen in Figure 1.2. The planar isomer represents the stable configuration, whereas the 3D structure is 0.27 eV higher in energy. Interestingly, the 3D structure is magnetic as it has two unpaired spin states. This indicates that the same size of cluster could have completely different chemical and physical properties. By knowing these structures, electrical and optical properties can also be determined.

In reality, larger size clusters involving a few hundred atoms are too big to analyze by spectroscopic methods, and yet are also too small to analyze with diffraction methods. Determining the structures of atomic clusters is difficult, as they have unusual, low-symmetry, or non-crystalline shapes. Therefore, a computational approach is currently the only way to predict the structures of the cluster.

1.3 Experimental Methods

Atomic clusters can be generated under specific experimental conditions, involving a few different methods as explained below:

1.3.1 Cluster Synthesis

There are several different methods of preparing clusters [4] [5] [6].

1. Laser vaporization: Mix metallic powders or single alloy rods are vaporized

by a laser beam. obtained

2. Ion Sputtering: The metal source is bombarded by the high energy inert gas ions such as Xe^+ .
3. Gas aggregation: A material from which clusters are needed are heated with temperatures high enough for evaporations, with the resulting gas propelled by an inert gas and cooled to allow the atoms to lose energy and form aggregates.

One of the most common ways to study clusters is through the use of molecular beams. Atomic clusters are transformed into gas forms through the vaporization of the cluster source. Throughout the vaporization process, the atoms exist as a gas phase. The atoms then start to form a cluster nucleus and grow by gathering additional atoms. At the end, the small newly-formed clusters start to merge together and eventually form larger clusters.

During the growth stage, the clusters are expanded by supersonic expansion because the clusters generally shrink due to the evaporation. Those clusters go through a narrow nozzle into a vacuum environment. At this stage, clusters are cooled and condensed until they become a narrow beam. In a molecular beam, clusters do not collide each other; therefore, their properties of clusters can be studied.

1.3.2 Characterization

Structural properties are difficult to characterize in atomic clusters through experiments because current technology does not allow for a direct method to characterize all properties. There are some indirect methods used to identify cluster properties when no direct method is available. Some of useful techniques are briefly mentioned below. It must be noted that there are currently no direct methods to get structural information of gas phase atomic clusters. Even though the diffraction technique has proven to be a useful technique, clusters are deposited on the insulating surface, thereby causing a structural change induced by the interaction with the insulator surface.

Mass Spectrometry

Mass spectrometry is used to measure the mass-to-charge ratio of charged clusters. The basic principle behind mass spectrometry is the molecular deflection of atomic elements. All atoms of the desired element are ionized before they are hit by a molecular beam. For example, hydrogen atoms are ionized and then hit by a molecular beam. As hydrogen is very light, large deflection occurs. In contrast, elements such as nitrogen are considered heavier in comparison to hydrogen, and predictably have a smaller deflection than with hydrogen. This demonstrates that mass of the desired element determines the magnitude of deflection. From the amount of deflection, speed of element and magnitude of beam force, the mass of the atomic clusters can be calculated. Moreover, it is possible to calculate the cluster size from the mass. The following is a basic procedure of mass spectrometry:

1. Ionization

The clusters are ionized by techniques such as laser ionization or electron impact. Loss of electron usually yield a cation. After the ionization, those ions are generally accelerated in order to have same kinetic energy.

2. Deflection

The ionized clusters are deflected by the magnetic field. The amount of deflection is strongly dependent on the mass of ions and the charge on the ion.

3. Detection

The sorted cluster ions are measured by the appropriate detector. When cluster ions hit the detector, an electronic current is produced. This current is then recorded and plotted as a function of mass and charge (m/Q), thus producing the mass spectrum.

It has to be noted that all processes must be operated under ultra-high vacuum conditions because the cluster ions could hit the molecules present in the air, therefore changing their composition and properties.

Diffraction

X-ray diffraction (XRD) is a powerful method to study the structure of larger atomic clusters. However, smaller clusters, such as 5-atom clusters are, too small for diffraction. X-diffraction determines the structural information and crystallinity of the atomic clusters. The basic principle of XRD is based on Bragg's law equation. The incident beam hits the surface and diffracts. At this stage, the diffraction angle can be obtained and wavelength should be known. By using Bragg's law, lattice spacing can be calculated:

$$2d \sin(\theta) = n\lambda \quad (1.1)$$

where n is an integer determined by the order given, λ is the wavelength, and where d is lattice spacing.

By using Equation (1.1), the bond distances of clusters can be determined.

As it was mentioned earlier, it is extremely difficult to determine the structural information of gas phase clusters. Electron diffraction method is one of the few options to analyze the gas phase clusters. However, the experimental results are very complicated and makes it difficult to determine the exact structures. Rough information such as average cluster size and very rough geometry information, though, can be acquired.

Transmission Electron Microscopy

For supported clusters, Transmission Electron Microscopy (TEM) is a very useful technique compared to other microscopy techniques such as scanning electron microscopy (SEM) due to its penetration ability. SEM is good to use for bulk materials because of its topographic ability. The principle of TEM is that incident electron beam transmits through the samples. During the transmission, those electrons interact with the samples. As a result, the image shows a contrast of electron interaction. The advantage of TEM in the cluster study is to its ability to provide internal information of nanoparticles. It could be possible to see periodicity of nanoparticles if the cluster size is very large.

1.4 Metal Clusters

1.4.1 Ruthenium

The ability of Ruthenium to harden platinum and palladium, as well as its lower cost of production in comparison to rhodium, makes it a highly useful element when constructing alloys for wear-resistant electrical contacts. It is also used when constructing thick-film chip resistors. The presence of ruthenium in titanium alloys increases corrosion resistances. With applications also including turbine blades in jet engines, superconductivity of ruthenium-molybdenum alloys at temperatures lower than 10 K, and radiotherapy of eye tumors, ruthenium is a highly-useful metal.

1.4.2 Tin

Tin is especially useful for platinum-metal modifications, as it helps metallic nanoparticles anchor to supports in a uniformly-dispersed manner and increases catalytic behavior in the nanoparticle cluster[7].

1.4.3 Ruthenium Tin

Ruthenium-Tin is known as a very efficient catalyst for hydrogenation [8]. However, currently there are no effective experimental methods to establish the structural characterization of Ru-Sn clusters. A computational approach is currently the only method to determine their structural information. This is valid for all types of clusters.

1.5 Applications

1.5.1 Catalysis

Atomic metal clusters are highly sought after in catalysis studies because of their tuneability and reactivity. It is known that in some cases, catalytic activity increases by alloying bulk metals. This similarly occurs for metal clusters [2]. In general, there are several reasons why clusters attract attention within catalysis:

1. Gold clusters catalyze oxidation reactions.
2. The catalytic activity of bimetallic clusters are, in some cases, much higher than their monometallic counterparts. For example, ruthenium is a good hydrogenation catalyst by itself, but mixing with tin increases its performance [2].
3. Ruthenium and copper are immiscible in bulk states. However, they are miscible at the cluster level and are good hydrogenation catalysts.

This shows us that it is possible to tailor a desired catalyst by mixing two different metals.

1.5.2 Magnetic Applications

Aggregates of atomic clusters, when inside nonmagnetic materials, exhibit giant magneto-resistance with a variance in resistance of 50% when an external magnetic field is applied [9]. Due to this property, there is the potential to increase the storage space of a hard disk drive.

1.5.3 Hydrogen Storage

Hydrogen storage has caught a considerable amount of interest during the past few decades due to its potential use as an energy carrier. It has been shown some interesting results with the atomic clusters. Magnesium hydride is known for high hydrogen absorption materials. However, they require high temperature to reverse the process. Small magnesium clusters can release the much more hydrogen than their bulk because the average number of bond is less than bulk so that desorption energy is very low [10]. As a results, hydrogen can be reversed in low temperature with MgH_2 clusters. Besides Mg clusters, aluminum clusters can be able to absorb more hydrogen than their bulk because their surface to volume ratio of small Al clusters increase with decreasing the cluster size [11]. Thus, unique properties of atomic cluster could bring great results on hydrogen storage field.

1.5.4 Biagnostics

Nanoparticles are especially useful for biodiagnostic applications such as cellular labelling and DNA/protein markers. Specially tailor-made nanoclusters can increase the sensitivity and the selectivity of the marker, therefore increasing its ability to detect the presence of DNA or protein. An example of this is an application of Ag particles to Au particles, which proved to amplify a target signal and detect the desired substances as low as 100 aM.

Chapter 2

Theoretical Background

2.1 Potential Energy Surface (PES)

In order to understand atomic clusters, their atomic configurations must be known. In the coupled Basin-Hopping/DFT global optimization algorithm developed within this project, the potential energy surface (PES) is based on the Born-Oppenheimer approximation. The Born-Oppenheimer approximation is the assumption that, when calculating the wavefunction of a molecule, electron and nuclei are treated as separate entities. Since the mass of the nuclei is considerably heavier than their electron counterparts, they are considered stationary, allowing for the electrons to freely move around the nuclei. Thus, the PES is determined as a function of the cluster atomic positions. This means that the energy of the system can be calculated from the number of atoms and their configurations. Simpler interatomic potentials such as Lennard-Jones could also be used in order to rapidly explore a nanoparticle PES; nevertheless, the accuracy of the simulation can be compromised. Details of the Lennard-Jones potential are explained below.

2.2 Lennard-Jones Potential

The Lennard-Jones potential is a simple mathematical model for approximating the interaction between atoms. Although this potential is not very accurate, it

is still used because it is convenient and time-efficient. It was used in the early stage of the project, as there is much data available where the Lennard-Jones potential has been used, making it convenient for making comparisons during the development of the code.

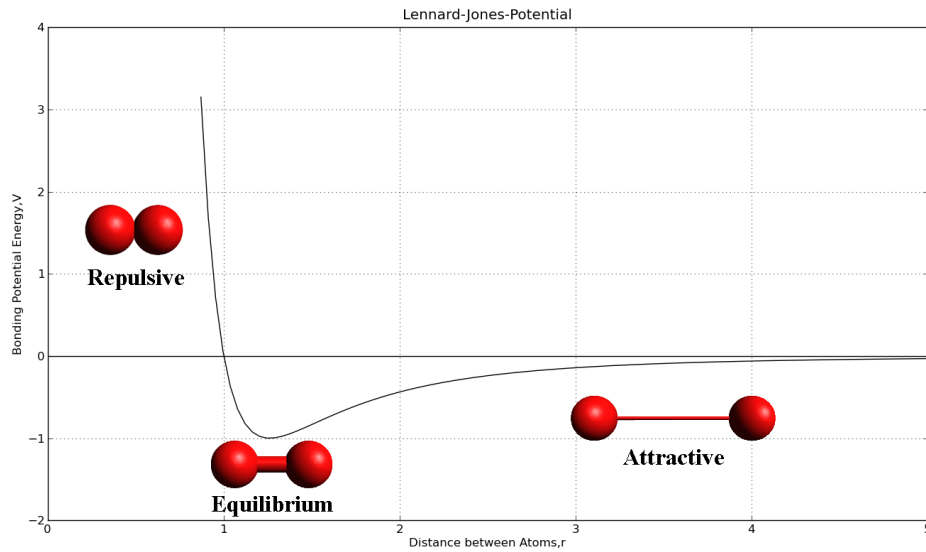


Figure 2.1: The Lennard Jones Potential.

The basic idea of Lennard-Jones potential is simple. The energy in the LJ model is expressed as the equation listed below. The relation between bonding and potential energies are plotted in Figure 2.1 and was calculated by using Equation (2.1).

$$E = 4\epsilon\left(\left(\frac{\sigma}{r}\right)^{12} - \left(\frac{\sigma}{r}\right)^6\right) \quad (2.1)$$

E is the potential energy between the atoms. σ represents the distance when the potential is zero. ϵ is the depth of potential well. The first part, $(\frac{\sigma}{r})^{12}$, represents the repulsive force and the latter one, $(\frac{\sigma}{r})^6$, represents the attractive term.

Figure 2.1 represents typical LJ potential graph. Assuming that there are two infinite separated atoms. At this situation, the bonding potential energy is zero.

As the distance between atoms decreases, their potential energy increases. Eventually, they are bonded and reach an equilibrium point, which is characterized by the lowest potential energy. If the two atoms are pushed together after reaching the equilibrium point, they start to repulse each other due to the Pauli exclusion principle. According to this principle, no two electrons in the same system can be in the same quantum state. It must be noted that potential energy starts to increase once it passes equilibrium point and atoms begin to repel each other.

2.3 Density Functional Theory

Nowadays, Density Functional Theory (DFT) is probably the most-used ab-initio methodology in condensed matter physics and material science. The basic principle of DFT is that energies and properties of ground states can be calculated from the electron density. Individual particles are treated as a function of its atomic coordinates, which are represented as X, Y, and Z in the many-body system. The many-body system means that there are a large number of particles interacting with each other. The Schrödinger equation is able to solve wavefunctions with one electron; however, it is unable to solve many-body systems.

In order to solve many-body systems, some approximations need to apply to the Schrödinger equation. DFT originated from 1964, when Hohenberg and Kohn proved the total energy of a system can be calculated from the function of the electron density[12]. Later, Kohn and Sham proved that the ground states of the system can be calculated by one electron schemes[13]. Reducing the parameters that describe the many body system has been the goal of DFT. After many years of development, DFT has also become a useful method in computational chemistry. However, there are some disadvantages. One is that DFT is an extremely time-consuming process. Therefore, the aid of a super computer is generally required for DFT calculations of nanometer-sized systems. However, this is still a big issue for global optimization problems. It could take years to find the right structure in large systems which contain thousands of atoms. Therefore, the approximation potential system can be usefull to understand the large system until the arrival of a next-generation supercomputer. The Lennard-Jones potential has good approximation for noble gas systems.

2.4 Cluster Relaxation

Atomic relaxation in physics and chemistry means to find the equilibrium states from a nonequilibrium system. There are many relaxation algorithms. In the project, three common relaxation algorithms are presented: Broyden-Fletcher-Goldfarb-Shanno (BFGS), Limited Memory BFGS (L-BFGS), and Fast Inertial Relaxation Engine(FIRE). The BFGS method is a class of hill-climbing optimization methods. In L-BFGS, the Hessian Matrix is inversed. This method is useful when there are many variables in the system. Fast Inertial Relaxation Engine (FIRE) is a faster method compared to BFGS [14]. The process consists of one simple equation. The result is not as accurately as BFGS but it gives one a good approximation of global minimums. Since it is fast and bring goods results, this could be used for Basin-Hopping with Lennard-Jones clusters for fast calculation of monometallic and bimetallic clusters.

2.5 Energetic Analysis

2.5.1 Atomic Unit

The electron volt,eV,an energy unit generally used in quantum mechanics, is the energy than an electron has after the electron is accelerated by 1 volt. However, the atomic unit Hartree is often used with software such as Dmol.

The unit Hartree represents the potential energy of a ground-state hydrogen atom. The unit can be converted to electron volt for convenience.

$$1 \text{ hartree} = 27.31138 \text{ eV} \tag{2.2}$$

However, it is much more convenient to convert to an electron volt because the energy difference between the local minima is very small.

2.5.2 Binding Energy

Energetic analysis is an important role in analyzing the cluster from a theoretical point of view. Total energies are mainly used to compare the energy difference

between the local minima. However, total energy varies depending on the different DFT approximations. Instead, the binding energy is used. Binding energy is the energy necessary to separate the aggregate atoms to individual atoms. A larger binding energy means the bonds between the atoms are strong. The binding energy of one element is simply calculated by equation (2.3):

$$E_b(A_X) = E_{Tot}(A_X) - X E_{Tot}(A_1) \quad (2.3)$$

To analyze the binding energy, plotting is needed. The Y axis is defined as $\frac{E_b}{N}$. N represent number of atoms. The X axis is defined as $(\frac{1}{N})^{\frac{1}{3}}$ for an easier analysis. Such a graph would demonstrate how clusters evolve through increasing the size of clusters. Point zero in the graph is bulk value.

For bimetallic system, the binding energy is calculated by two possible different equations (2.4) or (2.5).

$$E_b(A_X B_Y) = E_{Tot}(A_X B_Y) - X E_{Tot}(A_X) - Y E_{Tot}(B_X) \quad (2.4)$$

or

$$E_b(A_X B_Y) = E_{Tot}(A_X B_Y) - X E_{Tot}(A_1) - Y E_{Tot}(B_1) \quad (2.5)$$

Also, the binding energy of hydrogen is Ru-Sn, Ru, and Sn systems are calculated because experimentally it is known that hydrogenation of bimetallic systems is much stronger than single-element systems. Equations (2.6) and (2.7) are used to calculate the binding energy of hydrogen.

For bimetallic system,

$$E_b(H) = E_{Tot}(A_X B_Y H) - E_{Tot}(A_X B_Y) - \frac{1}{2} E_{Tot}(H_2) \quad (2.6)$$

For monometallic system,

$$E_b(H) = E_{Tot}(H A_X) - \frac{1}{2} E_{Tot}(H_2) \quad (2.7)$$

2.5.3 Vertical Electron Affinity

Vertical electron affinity (VEA) is the ability to form negative ion states from neutral states. VEA is calculated by Equation (2.8).

$$VEA = E_{Tot}(A_X(Neutral)) - E_{Tot}(A_X(Anion)) \quad (2.8)$$

It has been noted that neutral states here do not mean the structural ground states. First, total energy of the ground state of the anion is calculated. Then, the total energy of neutral states is calculated by changing the charged state of anion.

2.6 Distance Analysis

Besides the energetic analysis, the mean distance of the clusters need to be calculated. Every distance between the atoms in the structures is calculated. However, some distances are very large, an example being 5.0 Å. This is obviously too large for the system like Ruthenium or Tin because their average distance between the atoms is approximately 3.0 Å. Therefore, these large distances need to be ignored when calculating the mean distance. A graphical representation is also used in this case. The X axis is the number of atoms, where the Y axis is mean distance. The graph shows how the average bond distance evolves.

2.7 Electronic and Magnetic Properties Analysis

Electronic properties can be analyzed by inspecting the Kohn-Sham spectrum, which is obtained in the DFT calculation. An important electronic property is the HOMO-LUMO separation. It is very interesting to see how the binding energy of clusters changes as they evolve. Large HOMO-LUMO separations often designate high stability. From the HOMO-LUMO separation and size graph, the magic number, which is the number of nucleons that makes a nucleus stable, of the cluster can be found.

Magnetic property is all depending on electron spin states. If there are not any unpaired electrons, the cluster are diamagnetic. If there are unpaired electrons, it is paramagnetic. DFT calculations provide the spin states from a spin polarization calculation. Therefore, magnetic property can be determined from number of unpaired electrons.

Chapter 3

Global Optimization Schemes

The lowest energy structures, also known as the global minima (GM), represent the stable geometric configurations of the cluster. Finding the global minimum is a difficult task because structures of atomic metal clusters are unusual and have low symmetry. Moreover, the number of isomers has been suggested to grow exponentially with system size as it can be seen in Figure 4.5. As there are no established experimental methods to find structures, a theoretical approach is currently the only method of determining them. Presently, there are two successful algorithms. One is the Genetic Algorithm (GA), while another is the Basin-Hopping (BH) algorithm, which is used in this project. Both of them have comparable efficiency to find GM structures.

3.1 Genetic Algorithm

The GA was first applied in atomic cluster studies by Hartke [15]. Later on, Deaven did the structural optimization of Lennard-Jones clusters through a GA [16]. The underlying principle of GA is natural evolution. The methodology is based on the Darwinian evolution process. Brief instruction of GA is well explained by Johnston [17]. At first, some possibly random structures as known as initial population are constructed. The structures are relaxed by a chosen relaxation method. Next, the energy of the previously relaxed structure is set as the criteria of fitness. The parameter, fitness, is a measurement of quality of

the structure. High fitness means lower energy. From there, fifty percent of the structure is taken as parents. Those selected parents are now randomly paired (mutation) and make new structures (next generation of structures). This whole evolution process is repeated until there is no further energy reduction. As a result, ground state structure should be found. Compared to the Basin-Hopping algorithm, GA is a relatively faster process. However, GA could have issues with bimetallic systems. With the bimetallic system, the position of the element causes energy differences. In the GA method, it is quite difficult to test the system that has same coordinate but different element positions. For the bimetallic case, the Basin-Hopping algorithm is a better option, as it allows researchers to explicitly account for atom-exchange, thus carefully mapping the cluster PES.

3.2 Basin-Hopping Algorithm

3.2.1 Overview

Basin-Hopping algorithms (BH) are one of the most sophisticated global optimization techniques based on the Monte Carlo method. Wales and Doye proved the efficiency and accuracy of BH by using Lennard-Jones clusters up to 110 atoms [18]. The basic idea of BH is to generate a new cluster structure and relax it at every step. The energy of each relaxed structure is called local minimum and the lowest energy structure from those local local minimums are now called global minimum (GM). However, the BH algorithm does not guarantee to find the global minimum of the system. For instance, larger cluster sizes have a lower probability of reaching the global minimum than compared to smaller clusters because the combination of atoms increases exponentially when the number of atoms are increased. Therefore, the number of steps must increase in order to increase the probability of finding the global minimum.

3.2.2 Monte Carlo Method

Basin-Hopping is primarily based on the Monte Carlo algorithm (MC). MC is based on the idea of repeated random sampling in order to calculate results for

a specific problem. It does not guarantee the correct result, but statistically should reach the right result. MC can be used to simulate a variety of physical and mathematical phenomenon: for example, electron beam distribution of scanning electron microscopy, simulating turbulence flow and even in finance field to analyze investments and stocks.

3.2.3 Metropolis-Hastings Algorithm

The Monte Carlo Metropolis algorithm is the method used to collect random samples from the probability distribution where direct sampling is difficult. The method was first introduced in 1953 by Metropolis [19]. The principle of the Metropolis method provides two possibilities for every step in the Monte Carlo method. One is the acceptance of the step. Another is rejection of the step. Details can be explained by assuming that the system has the energy, E_{Start} and the “new“ energy E_{New} resulting from the random sampling. The acceptance of the system is now dependent on the sign of the energy difference. The probability, P , that a new system is acceptable is expressed by Equation (3.1).

$$\begin{aligned} P &= 1 \text{ if } \Delta E \leq 0 \\ P &= e^{-\frac{\Delta E}{k_B T}} \text{ if } \Delta E > 0 \end{aligned} \quad (3.1)$$

where k_B is the Boltzmann constant ($8.617343 \times 10^{-5} \frac{eV}{K}$), and T is the absolute temperature. Absolute temperature can be changed so that probability can be controlled. In other words, probability is very much temperature sensitive. Increasing the absolute temperature increases the probability when ΔE has positive sign. Therefore, Equation shows that the system is always accepted if the new energy is lower than the previous energy. Otherwise, the probability is dependent on the magnitude of energy difference and the absolute temperature, T .

3.2.4 Methodology

Here, the methodology of the BH algorithm is explained as follows:

1. Random structure is constructed. The distance between atoms in the cluster

is set according to the nearest distance allowed, which is dependant upon the elements being used.

2. The cluster structure is relaxed by an appropriate method such as DFT or Lennard-Jones potential. The total energy of the relaxed structure corresponds to a local minimum. Structure and energy information are both recorded.
3. The relaxed structure is completely taken out of its local minimum (destroyed) by an appropriate move strategy such as "shake". The new resulting structure is relaxed again.
4. The Metropolis-Hastings method is used in order to decide whether or not to accept the new cluster structure. If the new energy is lower than the energy of the previous structure, then probability is 1 and is automatically accepted. If the new energy is higher than the previous one, then the probability is based on Equation. In the case of the latter situation, the step is accepted if the probability is greater than a random generated number from range 0 to 1.
5. Points 1-4 are considered as one step within the simulations. Furthermore, in order to search for global minima structures, points 1 through 4 were repeated for 100 and 500 BH steps (see Figure 14).

Figure 14 shows step 1-4.

Figure 3.2 is complete basin-hopping method for 4 steps. Global minimum are located after 4 BH "shake" moves. As each local minimum region looks like a basin and energy moves to next basin, the method was named Basin-Hopping.

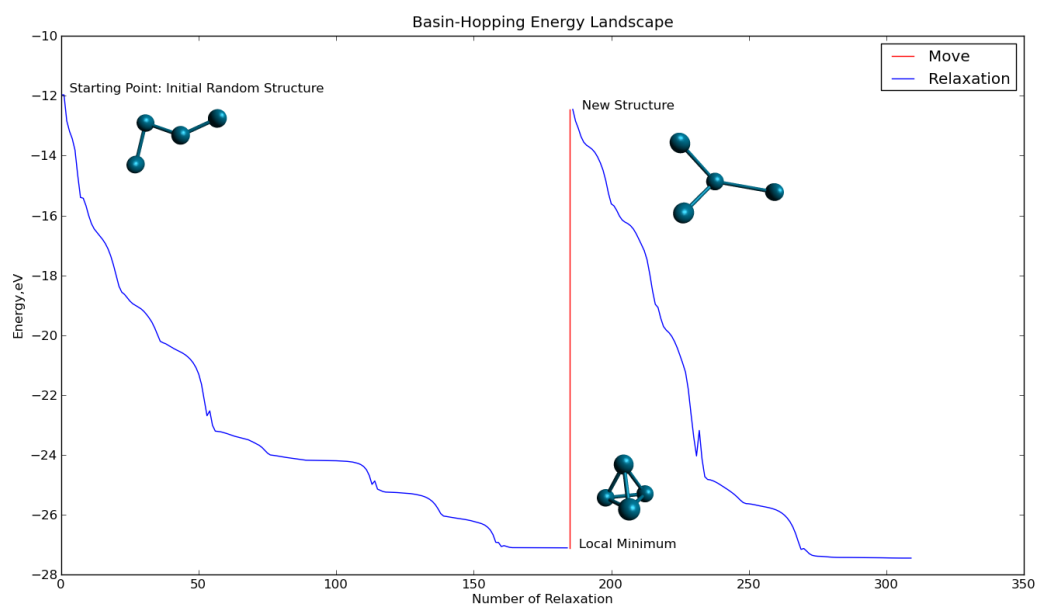


Figure 3.1: Example of a Basin-Hopping step.

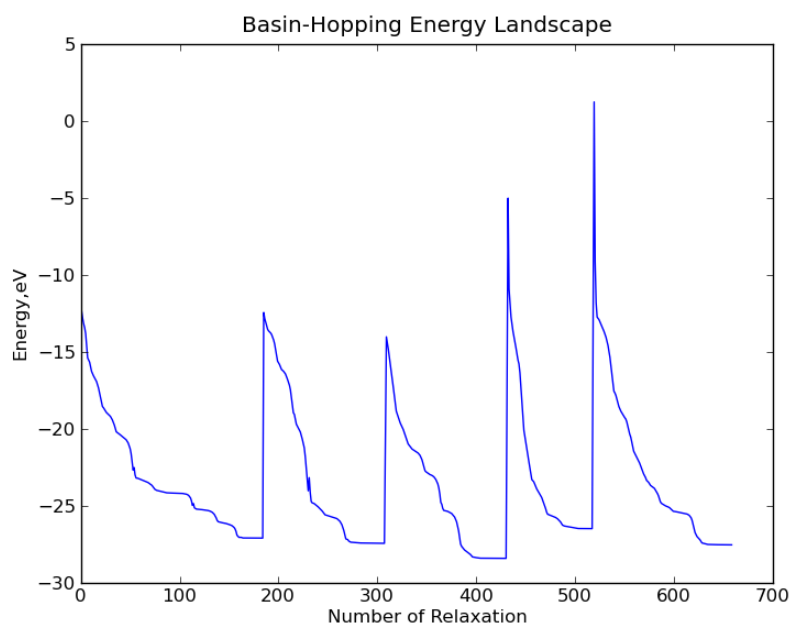


Figure 3.2: Basin-Hopping energy landscape.

Chapter 4

Methodology

4.1 Tools

The code for this project is written in Python. Python is one of the most powerful programming languages up to today. There are other options such as MATLAB and Fortran. MATLAB is very good at numerical simulation but it is extremely expensive, both computationally and economically. Most DFT softwares are still written in Fortran, as it is efficient for scientific computing. However, Python code is much more simpler than Fortran. Python code can be easily read by the users even they do not know the Python syntax, making it easier to share with the scientific community. In this project, Python is also used to process massive data and text processing. Python simplifies programming as it provides a lot of basic scientific modules as default. Moreover, Python is open source and is free of cost. Besides Python, all other tools in the project are also open source software with the exception of Dmol. The main softwares that are used in the project are mentioned in this section.

4.1.1 Atomic Simulation Environment

Atomistic Simulation Environment(ASE) is used to simulate atomic cluster structures [20]. ASE is part of the Python module. It is very suitable for this project because it has already contains basic modules which can construct bulk and surface structures for a desired element or compound. ASE is also easy to couple

with many DFT software, such as SIESTA and Dmol.

4.1.2 Avogadro

One of the drawbacks of ASE is that it does not provide a good graphic interface for atom visualization. Therefore, Avogadro, a molecular visualization software, was selected as it provides good quality graphic images, as well as is very simple to use. All figures of atomic structures in the project are done by Avogadro.

4.1.3 Density-Functional Theory Softwares

There are many different type of DFT calculation softwares available. One must note that faster calculation speed is key with BH algorithms because it generates a new structure which must be relaxed at every BH step. Since BH requires quick relaxation for each step in order to save time, SIESTA and Dmol are used [21][22].

4.1.4 Supercomputer

DFT calculations require access to high performance computers. Therefore, the aid of a supercomputer is necessary. The supercomputer in the project is provided by Chalmers Centers for Computational Science and Engineering, which is one of six nodes that belong to the Swedish National Infrastructure for Computing centers. The supercomputer named 'SVEA' is mainly used in the project. It consists of 16 RAM for 1 node (which is equivalent to 8 core processors). Since the project is dealing with small number of atoms, only 1 node is used.

4.2 Simulation with ASE

4.2.1 Simulating Lennard-Jones Clusters

Wales and Doye have successfully found the lowest energy structures of Lennard-Jones clusters containing up to 110 atoms [18]. The lists of those global minimums are reported at Cambridge Cluster Database [23]. The database contains the *xyz*

coordinates of those GM structures. This project's code contains a function that reads the xyz coordinates from those files in order to visualize them by using ASE graphic user interface.

4.2.2 Construct Random Initial Structure for Monometallic Clusters

The next step is to write a routine code that generates initial structures of a single element cluster (i.e. monometallic code). The initial structures have to be generated randomly with certain constraints. The first atom is set at coordinate (0,0,0). Next, a new atomic coordinate has to be created. The code generates a random array of *xyz* coordinates in the range -1 to +1 Å. Depending on the type of element, the range can be adjusted. Python consists of 'type' which can be ASE atom function, list,tuple,array,string and dictionary. Interaction between those types are very tricky. Most of time, two different types are not interacting each other. For example, ASE atom function only accepts tuples. However, the 'type' of atomic positions are first written by 'array'. Therefore, atom function does not take array as position so that array is converted to a tuple. The coordinate is the added to the initial coordinate at (0,0,0).

The code then generates a new randomly-generated atom and continues to add them to the system until the requested number of atoms is fulfilled. However, there are important conditions that have to be considered. The distance between atom must not be too close or too far. The distance between the atoms is based on $\sigma = \epsilon = 1$. Therefore, the code checks if the distance between atoms are above 1.0σ and less than 1.3σ every time new atoms are added. The constraining distance is changeable depending on the type of elements. If the new atom does not satisfy the distance condition, the new atom is discarded and new random coordinate is generated until it satisfies the condition.

4.3 Basin-Hopping Code

4.3.1 User Input

At this stage, the BH code is now constructed with aids of Python and ASE. At first, user changeable parameters are defined. Temperature, which is expressed as absolute temperature is an important role in Monte Carlo algorithm because it affect probability of accepting each step or not. The type of relaxation method can be chosen by the user from FIRE, BFGS and LBGS [14][24]. "Step-width" is also crucial, as it determines the range of distance that atoms can move during the move stage. "Step-width" can be also selected by the user.

4.3.2 Energy Function

During the optimization, energies are calculated based on calculators that was chosen by users. For instance, energy is calculated by the Lennard-Jones potential or DFT, if the calculator is set to any of these options. The calculator here means the way to sample the PES. At every relaxation step, total energies are calculated until the cluster structure reaches equilibrium state. The trajectory file is also created for each local energy minimum. The trajectory file corresponds to the Python ASE module and it can be easily converted to .xyz or .pdb files to be read using other molecular visualization software.

4.3.3 Move Strategies Function

There are two efficient move strategies implemented within the code: "shake" and "swap". The idea of the "shake" move is that every single atom in the system are displaced at same time. According to Rossi et al. [25], "shake" is the most efficient of the move strategies. In fact, the "swap" move does not work with a single element cluster because swapping the same element does not affect the cluster structure. Therefore, random *xyz* coordinates are generated in the "shake" move. The *xyz* coordinates are multiplied by "step-width" so that the overall magnitude of the atom movement can be regulated. Finally, these coordinates replace the previous ones. As a result, a completely new *xyz*

coordinate set is obtained.

The "swap" move is most effective in binary and ternary clusters because different elements in different position make a complete difference in the cluster total energy as well as its location in the PES. Two atoms are randomly chosen. If the same atoms in the "swap" move are chosen, the process is redone until the code finds a different atoms.

Beside these two movements, other movements are also created to increase the randomness. One is named 'hybrid move', where "shakes" and "swaps" occur simultaneously. The code accounts for this by having the "swap" movement to occur right after the "shake" movement. Another strategy is that after every tenth "hybrid" move, only "swap" movements are carried out. The code accounts for this by defining the two moves as two different functions.

4.3.4 Run Function

The run function is created in order to start the BH algorithm. In this code, the position and energy of starting point are calculated. From here, the starting coordinates are displaced by a "shake" or "swap" movement and the total energy then calculated by an energy function (e.g. LJ or DFT). If the new energy is lower than the energy of the starting point, it is then automatically accepted and the previous structure is replaced with the new one. This prevents having a higher energy structure at each step during the BH runs. If the user wish to accept higher energy structures, then temperature can be simply increased so that probability to accept the higher energy structures increases. It has to be noted that the code overwrites the energy and its structural information every time a lowest energy structure is found.

4.3.5 Flow Chart for Basin-Hopping Code

All necessary functions for the BH code have been written and are shown in Figure 4.1 below.

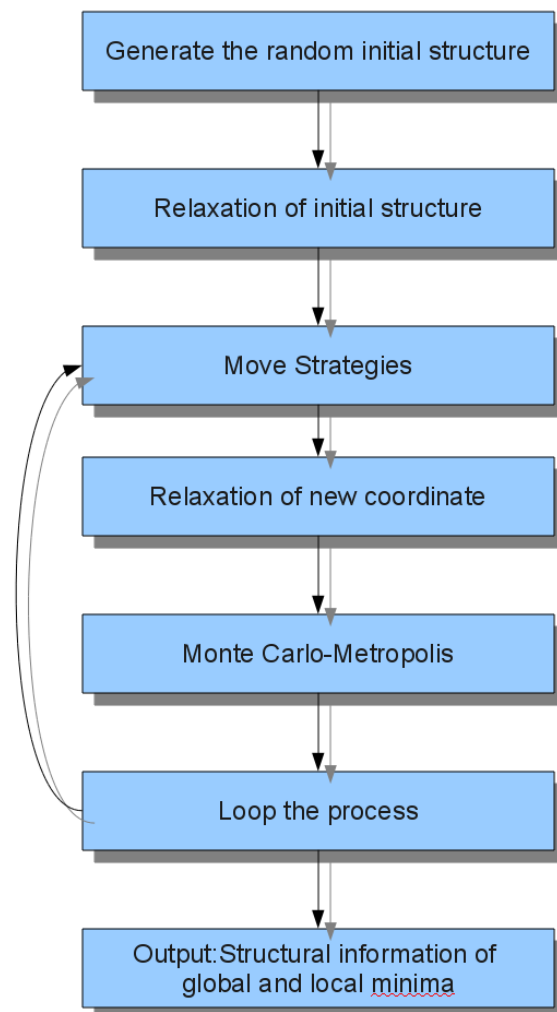


Figure 4.1: Schemes for the Basin-Hopping method.

4.4 Test with Lennard-Jones Potential

The Basin-Hopping code was tested for Lennard-Jones clusters in order to confirm that the code is able to work. Since LJ clusters are represented by a simple potential, it does not take time to run for small cluster size, even on a desktop computer. Lennard-Jone clusters for monary and binary systems are shown in this section. The results are compared against at the Cambridge cluster database.

4.4.1 Single Lennard-Jones Clusters

Lennard-Jones clusters up to 20 atoms were successfully reproduced by the BH code and compared against those found by Wales and Doye [18]. LJ clusters with $\sigma=1$ and $\epsilon=1$ are chosen. The number of BH steps for each process is set to 100. Step-width is set to 0.5. The results are summarized in Table

Number of Atoms	This work / ϵ	Wales/ ϵ	Point Group
5	-9.1038260	-9.1038520	D_{3h}
6	-12.711983	-12.712062	O_h
7	-16.505307	-16.505384	D_{5h}
8	-19.821446	-19.821489	C_s
9	-24.113308	-24.113360	C_{2v}
10	-28.422445	-28.422532	C_{3v}
11	-32.765864	-32.765970	C_{2v}
12	-37.967464	-37.967600	C_{5v}
13	-44.326669	-44.326801	I_h
14	-47.845109	-47.845157	C_{3v}
15	-52.322527	-52.322627	C_{2v}

Table 4.1: Total energies for LJ clusters.

4.4.2 Binary Lennard-Jones Clusters

Since the project is dealing with bimetallic clusters such as Ru-Sn, the code has to be able to generate random structures for binary clusters. The code which

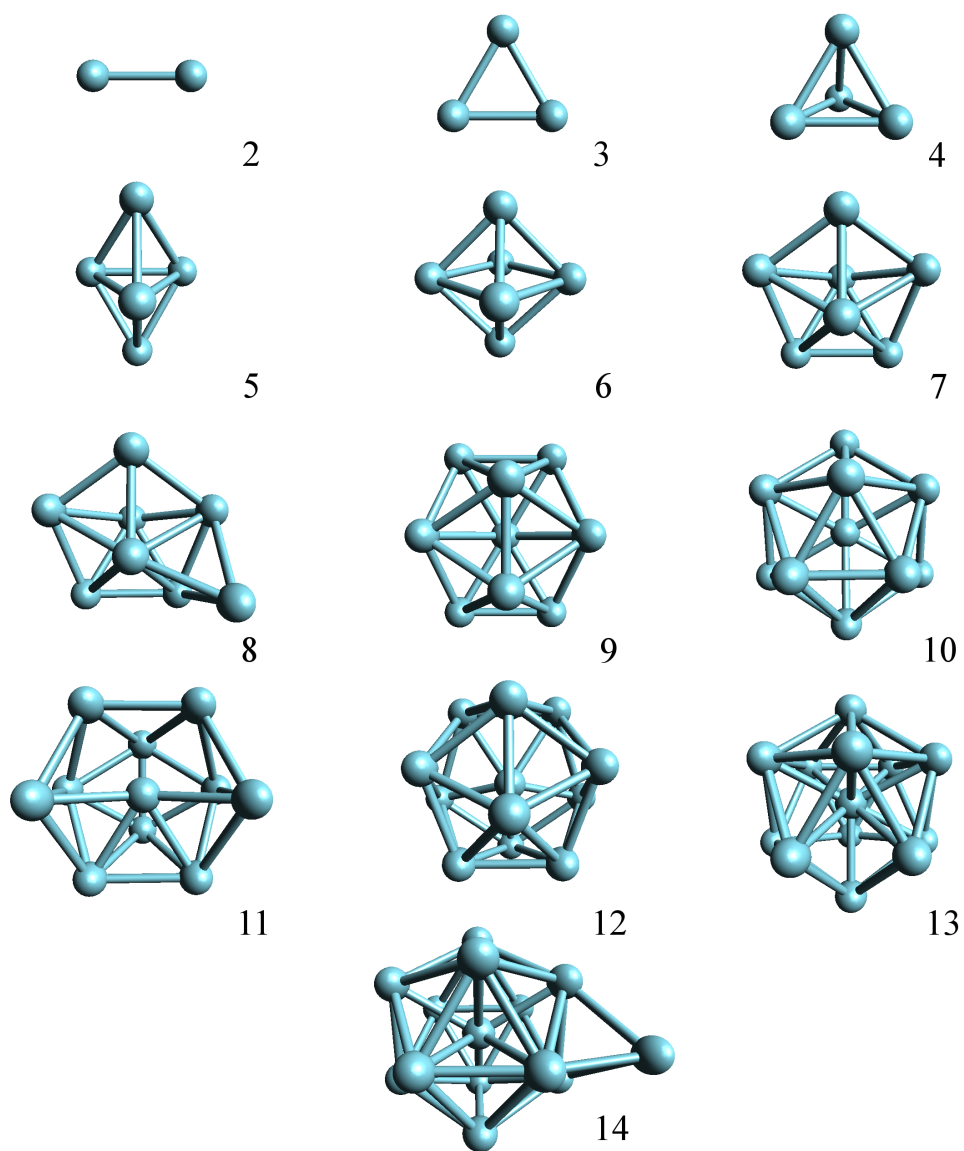


Figure 4.2: Structures for Lennard-Jones clusters obtained with the Basin-Hopping method.

is used in producing random single element structures is then simply modified. First of all, the number and type of each element can be defined through user input. Element lists are created according to the number of each element. When random coordinates are chosen, random elements from created element lists are randomly chosen. It means that coordinate and elements are both randomly determined. If the new coordinate is not too far or too close, the new coordinate and its element are added. If it does not satisfy the distance condition, the atom is deleted and the same process is repeated. Once the new atom is added, the element is removed from the element list so that the code does not pick the exact same element again. After repeating the process based on number of atoms and their element, a random binary structure are constructed.

The Lennard-Jones potential for binary clusters also has to be modified. Doye defines the following equation based on the Lorentz rule [26].

$$\epsilon = \epsilon_{AA} = \epsilon_{BB} = \epsilon_{AB} \quad (4.1)$$

$$\sigma = \frac{\sigma_A + \sigma_B}{2} \quad (4.2)$$

Thus, the Lennard-Jone potential defined in Equation (2.1) needs to incorporate parameters from Equations (4.1) and (4.2).

Therefore, the Lennard-Jones potential code has to consider three combinations. One is LJ_A-LJ_A with σ_A , while another is LJ_B-LJ_B and σ_B and finally LJ_A-LJ_B . When two atoms are of the same element, the Lennard-Jones potential for one element is used. The values of sigma are changeable by the users. When two atoms have different elements, σ is simply replaced by Equation (4.2). The ϵ value remains the same. In this case, ϵ is 1. The code checks the type of element and whether its combination is A-A, B-B or A-B during the calculation. Depending on these combinations, the code chooses the correct Lennard-Jones equation and calculates the potential energy. Once the Lennard-Jones potential code for the binary system was written, randomly-generated binary initial structures are able to be relaxed successfully.

In the BH code for the Lennard-Jones potential for binary systems, the value of σ is set to 1.1 and sizes up to 15 atoms is tested. 100 BH steps were chosen for

each cluster size. The corresponding optimized geometries and its corresponding energies are shown in Figure 4.3 and Table 4.2, respectively. Results were obtained similar to those reported by Doye [26]. Slight energy differences are due to the lack of BH steps. Interestingly, binary Lennard-Jones clusters tend to elongate around size 14 atoms, compared to monoatomic clusters.

Number of Atoms	This work / ϵ	Doye/ ϵ	Point Group
5	-9.1192430	-9.1193020	D_{3h}
6	-12.715190	-12.715734	D_{4h}
7	-16.556935	-16.557098	D_{5h}
8	-19.942861	-19.948687	C_1
9	-24.268611	-24.300649	C_{2v}
11	-33.388284	-33.371304	C_{2v}
12	-38.853496	-38.954245	C_{5v}
13	-45.360619	-45.543272	I_h
14	-49.040845	-49.049816	C_{3v}
15	-53.501576	-53.599281	C_s

Table 4.2: Total energies for Binary LJ clusters.

4.5 Evaluations Tools

Several evaluation codes were written in order to evaluate move strategies, optimization methods, structural analysis and structures by energy order.

4.5.1 Read Energy Code

The energy code read each local energy minima from output files which contains the number of steps, local energy minimum and lowest energy minimum up to the number of steps. The code was simply written to read specific lines of output files. Furthermore, the code allows for sorting the cluster structures by energetic ordering, i.e. an important feature to analyze these structures.

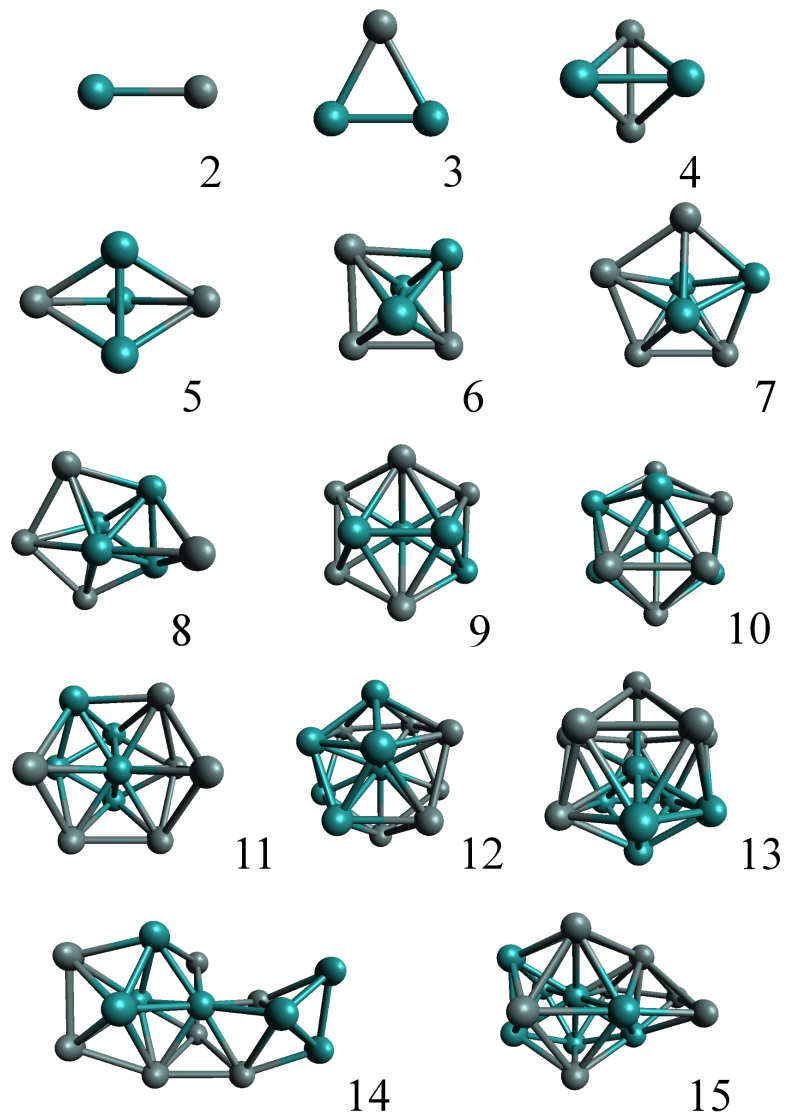


Figure 4.3: Structures for Binary Lennard-Jones clusters obtained with the Basin-Hopping method.

4.5.2 Histograms Code

To see how many local minima the BH reaches, the code generates a histogram of local energy minima. In this code, local energy minimum lists, created by the "read energy" code, are read as a string format. The data is then converted to a tuple and then further converted to a value. The histogram shows how many times the BH code visits each same minimum.

4.5.3 Bar Chart Code

The code creates a bar chart that shows the number of steps taken to reach the equilibrium states. The code counts the number of steps in each BH step. This bar chart is useful to make comparisons between different optimization methods.

4.5.4 Read Different Structural Coordinate Extension Code

In molecular design software, there are many different file formats for structure coordinates such as xyz files. The Python ASE environment generally uses the '.traj' format. When comparing the results against published data, other authors generally use a variety of different formats. Therefore, a code that can read any types of structural files such .xyz, .car and .pdb file extensions is necessary. These coordinates are also automatically converted to Python ASE atom functions.

4.5.5 Sort the Local Minimum Structures by Order of Energy Code

When the BH simulations finished, several hundreds of structures are saved as output. However, these structures are not sorted by order of energy. Additionally, there are many very small energy differences between structures that are considered as same structures. Therefore, a code that orders structures by energy and screens for duplicable energy is needed. In this code, all structures that are created during BH and all local energy minima are read. Each structure has to match with their corresponding energies. In order to do this, structures and their corresponding energies are paired by using the Python dictionary function.

During this step, duplicate energy values and their structures are automatically removed from the list. Once the code is executed, the output returns the energies and their structures in order of lower energies to higher energies. For convenience, the index tag and energy difference from the lowest energies are also shown.

4.5.6 Re-relaxation Code

Fine relaxations are needed once the BH process is finished. This code reads the lowest energy structures from a .traj file and can relax again with new input parameters such as a larger basis set and smaller thermal smearing of the occupations.

4.5.7 Measure Distance Code

Once these processes are complete, another code is implemented. This code automatically calculates all bond distances within the cluster and the average of all of them. This code basically reads re-relaxed lowest energy structures from the .traj file as well as measures all distances. In this step, the code also checks if two atoms are the same or different type, in order to distinguish distances between atoms of the same or different element. At the end, the code calculates the average distance of each element combination.

4.6 Move Strategies Analysis

Move strategies are carefully evaluated in this section. Four different move strategies are implemented. They are “shake“, “hybrid“ of shake and swap the different atoms, ”swap every 10” hybrid , and “shake every 10 hybrid”.

Analyzing move strategies is one of the key points, as it allows the code to get as many different structures as possible. One of the main differences between binary and monoatomic element systems is the move strategy when dealing with the Monte Carlo method. “Shake“ moves are commonly used due to its high efficiency [25]; however, this method has two drawbacks. One problem is its large CPU and time consumption. Every time the code finds local minima, structures are destroyed and moved to completely random coordinates. This new structure,

now in effect after the shake movement, could have much larger energy value depending on the "step width". This means that it takes a lot of time to determine an equilibrium state. In order to prevent this, the step-width has to be carefully chosen. A larger "step width" is ideal, but a big energy jump must be avoided. Another issue is randomness of the "shake" movement in binary system. As mentioned, different types of atomic elements causes energy differences. It is the best to add "swap" movement in the binary system in order to get as many local minima as possible. It has to be noted that within the single atomic element structure, swapping the same atom does not change its energy.

The results of using each of these types of movements are plotted as histograms. Simulations were run for each of these movements in order to compare results and determine the most efficient means of collecting the most accurate data. As seen from Figure 4.4, these histograms show the number of times local minima has been visited vs the total number of local minima. Table 4.3 shows the global minima, time to get global minima and the number of steps to achieve those global minima of each move strategies.

	Shake	Hybrid	Swap every10	Hybrid every10
Global Minima	-12.715669	-12.715682	-12.715664	-12.715606
Time	10min6s	9min16s	10min22s	2min8s
Steps to get GM	37	13	23	6

Table 4.3: Evaluation of move strategies.

The histograms in Table 4.3 indicate that the "shake" method and the swap every 10 hybrid steps method found the largest number of local minima out of the four methods. Finding as many local minima as possible is very important when it comes to much more complex cluster systems because it is important to know all possible isomers. The shake every 10 hybrid is particularly interesting, as it cannot find as many local minima as the other methods could, but it compiles 5-times faster than any of the three other systems. As a result, "swap every 10 hybrid" is the best choice here.

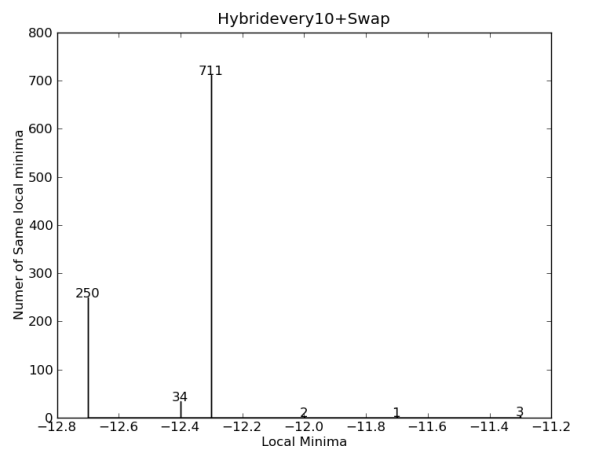
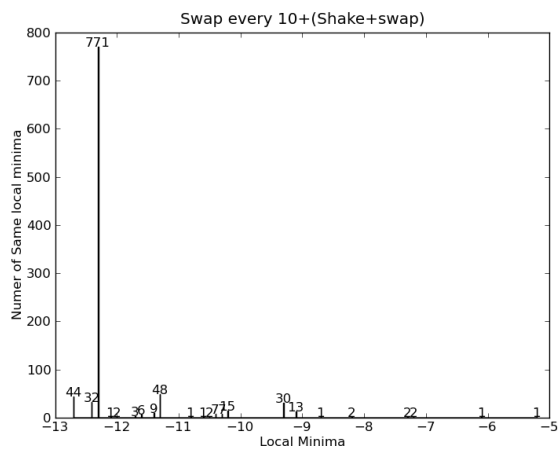
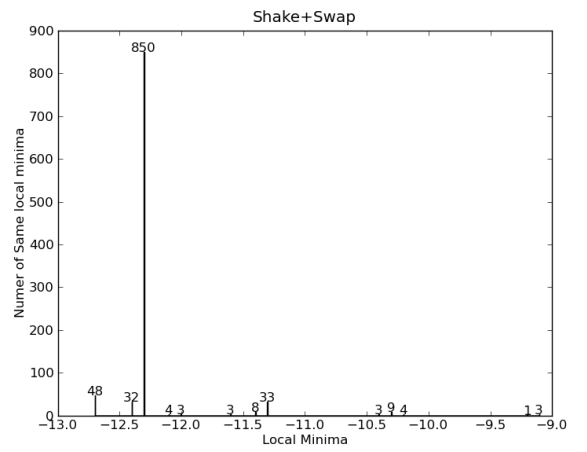
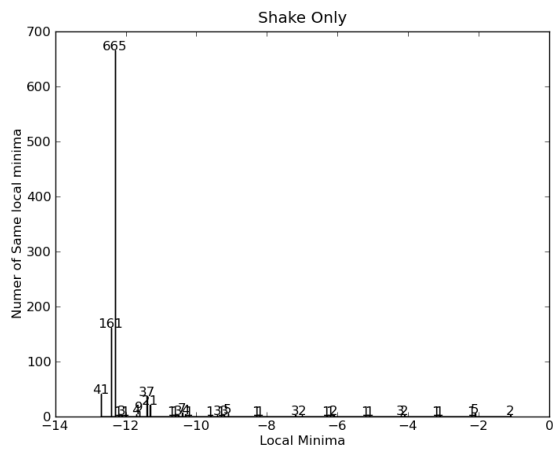


Figure 4.4: Histograms for number of found global minima

4.7 Relaxation Method Test

There are few different structural optimization methods in Python ASE environment: Broyden-Fletcher-Goldfarb-Shanno, (BFGS)[27], limited memory variation of BFGS, fast inertial relaxation engine (FIRE)[28]. The test was run for a binary system. The code generated a random binary structure which contains a total of 14 atoms. The same structure is used for all the tests because initial structures have to be the same in order to compare. The code thus reads the initial structure and relaxed by each optimization method.

N=14	BFGS	LBFGS	FIRE
Steps	197	294	450
Time	6s	9s	10s
Lowest Energy(eV)	-46.936798	-47.258899	-44.430068

Table 4.4: Comparison of different optimization methods.

Table 4.4 compares the lowest energy, number of steps, and time to finish, for each relaxation method. As Table 4.4 indicates, LBFGS found the lowest energy configurations among three of them. However, LBFGS takes approximately 100 steps more compared to BFGS.

4.8 BH Implementation in SIESTA

Lennard-Jones clusters were explored to ensure the BH code was working correctly. The next step was to move away from the Lennard-Jones potential and instead employ the DFT to get an accurate PES representation of the analyzed clusters. There are many different softwares available that use DFT, but for the purposes of this project, a program named SIESTA was used. It is an efficient implementation of the DFT calculations.

To start, a well-studied cluster with a known structure was needed to ensure the program was giving correct output once the code was modified to perform BH-DFT. Na_8 was chosen for this purpose, as it fulfills these prerequisites [29]. Sodium has a body-centered cubic structure (bcc) with a lattice constant of 4.29 Å. The structural factor of bcc is even so that position (110) may be chosen.

From this, the distance between the sodium atoms can be calculated by Bragg's law 4.3), resulting in a value of approximately 3.0334 Å.

$$d = \frac{a}{\sqrt{h_2^2 + k_2^2 + l_2^2}} \quad (4.3)$$

Therefore, a +/-20% range distance between sodium atoms is considered. In this way, initial structures, constructed by the project code, show that the distances between sodium atoms are of the order of 2.8-3.6Å.

The SIESTA calculations required a cell environment in order to perform periodic DFT calculations. The cell size cannot be too large or too small. A larger cell requires more time to calculate, making it time-consuming. Additionally, if the cell is smaller than the structure, SIESTA cannot make any calculations and would return an error. To account for this, a Na₈ cluster cell was placed in a cell with the dimensions 20×20×20 Å.

Within the cell, the randomly-generated structures were successfully relaxed when using the BFGS relaxation method. After this, a different mesh cut-off value and d and s set. It comes that the 160 mesh cut-off point is most stable and that the d set can have lower energy. Also, "step-width" and temperature (Boltzmann factor) are tested. "Stepwidth" at 0.8, 1.0 and 1.2 at constant temperature T = 100K are tested. Then, temperature at 50, 100, 150 and 200K with a constant "stepwidth" of 0.1Å is tested. Overall stepwidth of 1.0Å and a temperature of 150K are the best ones. "Step-width" of 1.2 Å found lower energy structures; however, it is very time consuming during the relaxation process.

BH with Na₈ was then performed once the previous steps were tested. However, the code could not find the global minima reported by Rothlisberger [29]. It turned out to be that the maximal force during optimization was set too high. To account for this, the maximal force is now set from 0.1 to 0.01 ev/Å. Once this change was done, the code successfully determined the global minima for Na₈. Figure 4.5 shows the different local energy minima structures for Na₈. Their energy difference is listed on Table 4.5. BH was run with 1000 steps to make sure to get all possible structures.

These results prove that the BH code performs really well when coupled with SIESTA.

Figure	Energy(eV)	Difference(eV)
1	-99.57	0
2	-99.45	0.12
3	-99.44	0.13
4	-99.42	0.02
5	-99.16	0.41
6	-99.01	0.15
7	-99.00	0.57
8	-98.91	0.09

Table 4.5: Na₈ energy differences.

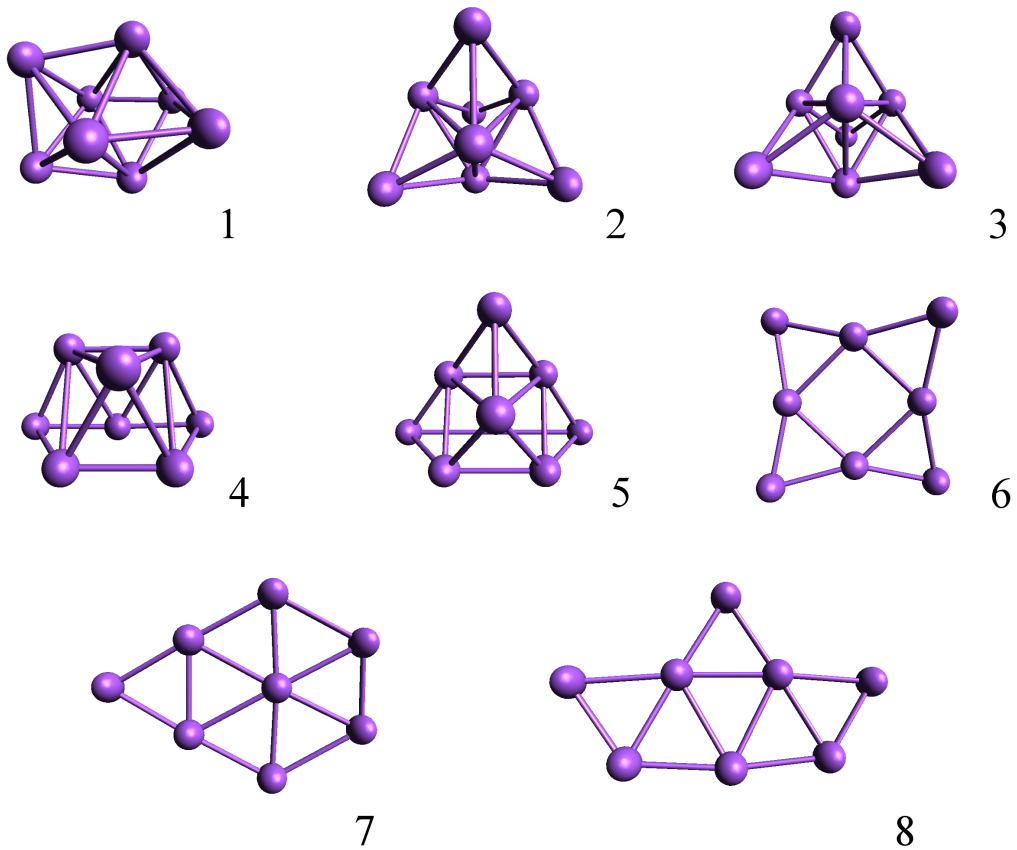


Figure 4.5: Optimized Na₈ clusters, where structure 1 corresponds to the global minima.

Ru-Sn clusters were also optimized by the BH code and SIESTA. During the relaxation process, Sn clusters were successfully relaxed; however, Ru clusters were not. The output files indicate that the total energy does not converge for Ru clusters. Within SIESTA, there are few parameters that are controllable by the user. While several tests were made using different parameters such as changing the mesh cut-off energy or basis set, none of them helped to converge the total energy. Exact reasons why SIESTA does not work with Ru clusters remains unknown. Therefore, alternative DFT calculators, such as Dmol, was considered.

4.9 Implementation of Dmol

Dmol is the default DFT calculator for the commercial software Materials Studios, which is owned by Accelrys. Dmol is an efficient implementation of the DFT and its efficiency has been proved [30]. Because of its efficiency and the speed of calculation, Dmol was used instead of SIESTA. However, the Python ASE environment does not support Dmol as a DFT calculator. Therefore, a script that accepts Dmol as a DFT calculator had to be written. The main purpose of this script is to convert Python atom coordinates to a .car file, which is a coordinate file extension for Dmol. The converted .car file can now be used to calculate the total energies of Sn, Ru, and Ru-Sn clusters. Then, the cluster structure coordinate file (.car) is then re-converted to a Python .ase file after each Dmol relaxation is done.

A code that converts from Python .ase to .car format was written. The code basically read elements and their coordinates and organize it as a .car file format. The code reverses the process in order to convert from .car to Python .ase format. The code that sends the .car file to Dmol is also made. The code simply sends the .car file to Dmol calculator, where it is relaxed with the BFGS method, and outputs the data that includes the total energy. All of the codes here are placed in get-energy function in the basin-hopping code.

Furthermore, Dmol has a lot of user input parameters. The lists below show tunable parameters. Only relevant parameters are described here.

- Opt-energy-convergence - Tunes the criteria for total energy convergence during optimization.
- Spin-polarization - Decides whether to perform a spin polarized calculation or not.
- Charges - Decides the charge state of system.
- Basis - Chooses the basis set.
- Pseudopotential - Chooses a potential to treat core levels.
- Functional - Specifies the LDA and GGA functionals to be used for exchange and correlation.
- Integration-grid - Decide the mesh point grid.
- Occupation - Control the temperature of the system so that orbital occupation can be controlled (electric smearing).

Relaxation using Dmol was firstly tested for the Ru_2Sn_2 cluster. The cluster was successfully relaxed by Dmol. The input parameters have to be tuned depending on cluster size and element, however, it indicates that Dmol deals well with Ru-Sn systems.

Chapter 5

Sn Clusters

BH was tested for Sn clusters up to 20 atoms. It is possible to run the test on cluster sizes of more than 20 atoms, but it becomes much more time consuming since the probability of finding the global minimum decreases when increasing the cluster size. Therefore, it is best to stop at 20 atoms. For comparison, the results are compared to those reported by Assadollahzadeh et al., [31]. The article shows the structures of Sn clusters of up to 20 atoms.

5.1 Basin-Hopping Sn Clusters

To start, the BH code was tuned. The “shake“ move was chosen because of single element cluster. The value of ”step-width“ was selected as 0.5 Å.

Input parameters for Dmol are, firstly, determined. Occupation was set thermal 0.03eV at first because metal clusters have a very small HOMO-LUMO gap. Therefore, a larger value was chosen here. The distance between atoms of initial structures for the BH code were set between 2.5 and 3.5 Å [31]. Tin clusters size from 2 to 10 were first tested.

However, the results did not compare to those reported by Assadollahzadeh et al., [31]. For example, the Sn₁₂ does not display a symmetrical structure [31], while a tetrahedral structure with symmetry was found as the lowest structure within the simulations. To confirm the structural differences between the project’s and Assadollahzadeh’s et al., results, structural coordinates files

were acquired from the author of paper. To compare the structural differences, both structures are again relaxed by the same input parameter of Dmol. As a result, the diamond-like structure has lower energy than the tetrahedron structure in Sn_{12} cluster. This indicates that the BH code is not working correctly.

After an investigation, it was found that the occupation values were set very high within the input parameters. Therefore, the occupation set the thermal value to 0.008 instead of 0.03. The BH code was then used to run the Sn_{12} cluster, with thermal value 0.008. As a result, the diamond-like structure became lowest structure and tetrahedron structure became second lowest. This indicates that occupation (i.e. electronic smearing) is a very important parameter when running BH with Dmol, because high temperature shifts up the virtual orbitals. Therefore, temperature must be set as low as possible in order to acquire the correct energy.

There is another important factor in BH-DFT with Dmol. BH is generally run approximately 500 steps for each cluster size. During this process, relaxation is the most time consuming process. Therefore, it is best to do faster relaxations in order to get as many structures as possible within the limited usage time allotted for the super computer. To do so, an integration grid is set as “coarse”. This means that computational time is faster but decreases the quality of the DFT calculation. The results regarding cluster geometries still remain to be trusted.

With those input parameters, BH was run for Sn clusters for sizes up to 20 atoms. The corresponding global minima of Sn clusters (up to 15 atoms) were successfully found. However, cluster sizes 16 to 20 had major issues with total energy convergence. For example, during the BH runs, unacceptable structures were generated, e.g. one of the atoms exists out of cluster aggregation or irregular shapes. These type of structural shapes induced an error in energy convergence. Once the total energy of a particular cluster did not converge, the BH code generates new coordinates from a structure that causes non-energy convergence. As a result, new structures start to spread and energy is never converged. This means that the BH code is not working anymore.

To prevent the problem, the BH code itself needed to be fixed because changing the input parameters does not solve the issues. In fact, input parameters such as occupation was tuned to converge the total energy but made it much more time

consuming; additionally the results were not trusted due to high temperature occupation. Therefore, the BH code was fixed. The most effective method was to reset the BH system every 100 steps depending of the size of the cluster. It means that the BH code stopped “moving“ the relaxed structures and generated completely random structure every 100 steps. In this way, energy can be converged again every 100 steps even when energy stops converging. With this approach, global minima for Sn clusters from 16 to up to 20 atoms were determined.

5.2 Relax the Selected Structures from Basin-Hopping Results

Approximately 5 cluster structures were chosen from the results because the BH code was not run with Fermi temperature, so there is a possibility that the lowest energy structure may not be the lowest when the structure is re-relaxed using Fermi temperature. In this step, relaxation must be strict. Therefore, few changes in input parameters are needed. The input parameters now used are:

- Optimal energy convergence: $1.0 \times 10^{-4} \text{eV}$
- Spin polarization: unrestricted
- Basis: dnp
- Pseudopotential: dspp
- Functional: pbe
- Auxiliary density: octupole
- Integration grid: fine
- Occupation: Fermi

In input parameters, occupation was set to Fermi, and the integration grid is set from ”medium“ to “fine”. However, total energy did not converge with Fermi in some of structures. Therefore, relaxations were performed using Thermal =

0.005. If the structures are relaxed with 0.005, then temperature is reduced to 0.001. At the end, relaxation with Fermi temperature was performed. In this way, all relaxations were successfully completed using Fermi temperature. The total energies of all relaxed structures were carefully compared and the lowest energy structures were chosen from Sn clusters from 2 to up to 20 atoms. Cluster sizes and their lowest energies are shown in Table 5.1 and Figures 5.1 and 5.2, along with Assadollahzadeh’s structures. The article structures were also re-relaxed with same input parameters as mentioned above.

Size	This work(eV)	Assadollahzadeh(eV)	This work,Anion(eV)
1	-3335.4280	No Data	-3336.08220
2	-6672.9289	-6672.9282	-6674.43600
3	-10011.7850	-10011.7882	-10013.3129
4	-13350.8726	-13350.8748	-13352.1654
5	-16689.6377	-16689.6380	-16691.4007
6	-20028.6751	-20028.6772	-20030.2988
7	-23367.6783	-23367.6698	-23369.3442
8	-26705.5775	-26705.5737	-26707.3310
9	-30044.5247	-30044.2631	-30046.4072
10	-33383.3762	No data	-33385.1561
11	-36721.1582	-36721.1019	-36723.2614
12	-40059.6742	-40059.4185	-40061.5478
13	-43398.1833	-43398.1831	-43400.3186
14	-46736.9890	-46736.9896	-46738.7455
15	-50075.5487	-50075.5201	-50077.7688
16	-53413.9824	-53413.9824	-53415.9961
17	-56752.2972	-56752.1954	-56754.5342
18	-60091.0562	-60090.7742	-60093.2418
19	-63429.2387	-63428.9346	-63431.4635
20	-66767.5677	-66767.5521	-66770.1352

Table 5.1: Comparison of Sn total energies.

5.3 Structural Analysis

Table 5.1 shows that Sn cluster sizes 7 to 13 and 15 to 20 have lower total energies than those reported in [31]. Moreover, cluster sizes 9,12,15,17 and 19 have

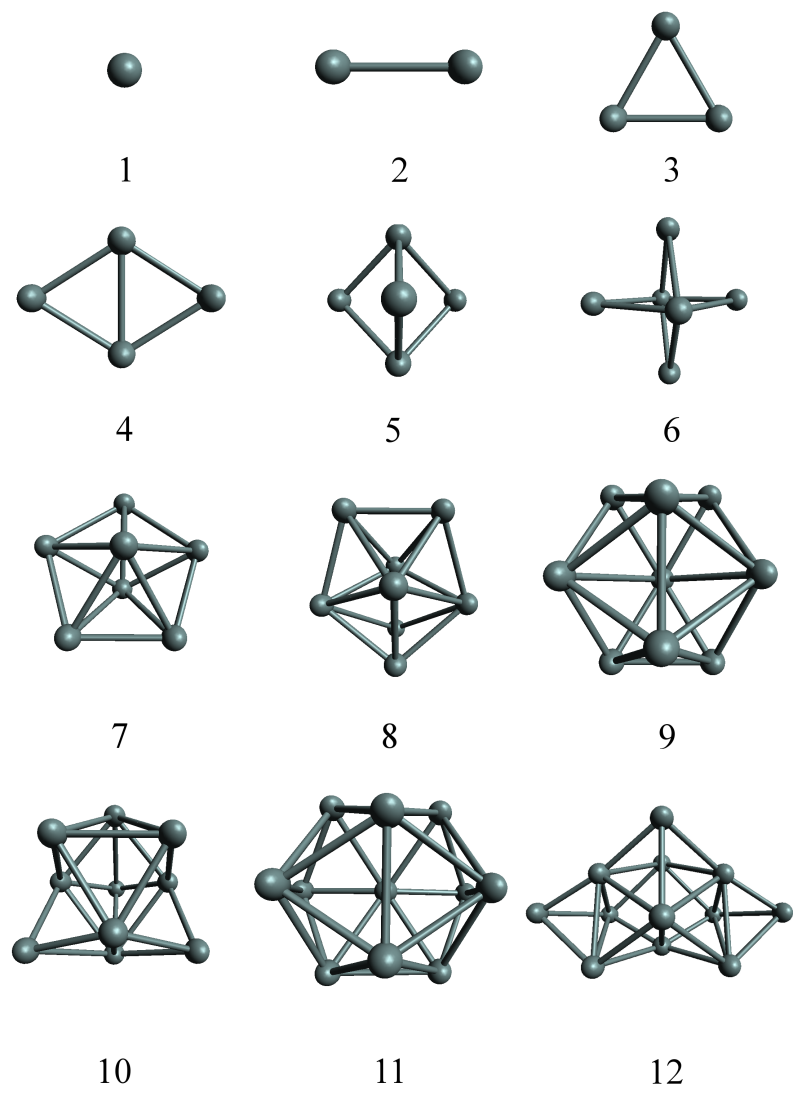


Figure 5.1: Ground States Structures for $\text{Sn}_1 - \text{Sn}_{10}$ clusters.

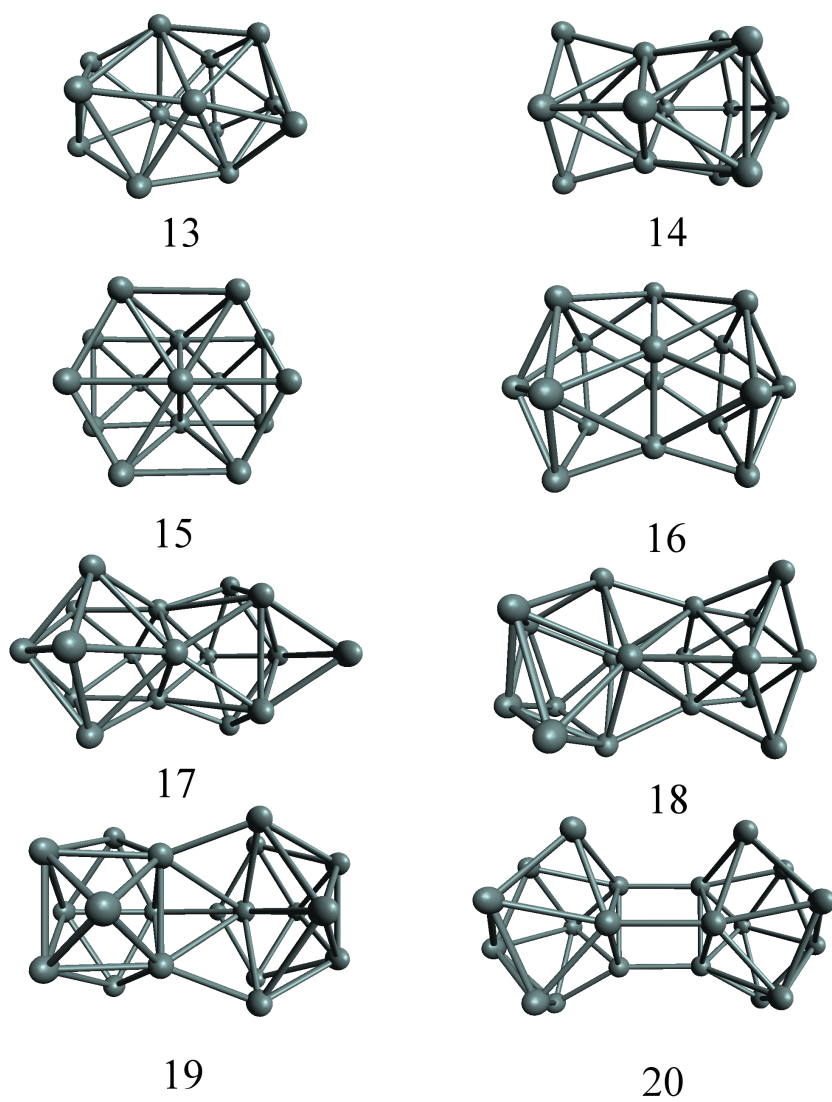


Figure 5.2: Ground States Structures for Sn_{11} - Sn_{20} clusters.

significantly different structures in comparison to [31]. Cluster size 18 and 20 have similar structures, but those found with the BH method structures have higher symmetry. Another interesting result is the elongation of the cluster structures. From Sn₁₆, the structures start to elongate. Eventually, Sn₂₀ clusters spreads to 2 aggregates of Sn₁₀ cluster each. They form the exact same structure.

The mean distance between atoms of each Sn clusters are measured by the “distance calculate“ program. Atoms are considered to be bonded if the inter-atomic distance lies between 2.5 - 4 Å. Table 5.2 shows the mean distance for each Sn cluster size; while the mean distance as a function of cluster sizes are plotted in Figure 5.3, Figure 5.3 shows that mean distance increases rapidly from size 2 to 8. Above 8, there are not significant changes.

Size	E_b (eV)	HOMO-LUMO gap(eV)	Mean Distance Å
1	0.00000	1.361	0.0000
2	-2.07278	1.669	2.8895
3	-5.50088	0.671	2.9402
4	-9.16042	1.061	2.9418
5	-12.49744	1.561	3.0051
6	-16.10685	1.575	3.1476
7	-19.68200	1.478	3.1053
8	-22.15316	1.001	3.2207
9	-25.67224	1.403	3.1647
10	-29.09569	1.774	3.2290
11	-31.44968	0.822	3.2239
12	-34.53767	1.585	3.1939
13	-37.61670	0.931	3.1784
14	-40.99638	1.267	3.1617
15	-44.12800	1.420	3.1545
16	-47.13371	1.328	3.1740
17	-50.02042	0.868	3.1732
18	-53.35141	1.159	3.1981
19	-56.10582	0.833	3.1792
20	-59.00674	0.491	3.1263

Table 5.2: Binding energy, HOMO-LUMO gap and mean distances for Sn clusters, from 1-20 atoms.

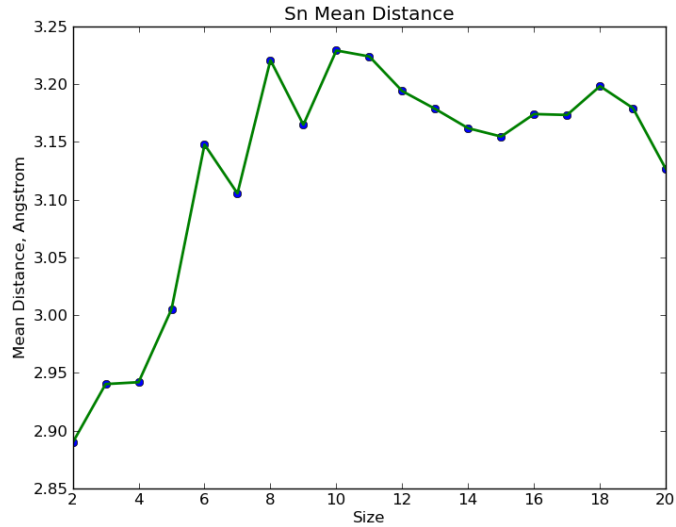


Figure 5.3: Mean distances of Sn clusters.

5.4 Energetic Analysis

5.4.1 Binding Energy

The binding energy of each Sn cluster was calculated from Equation (2.3). Binding energies of each cluster size are listed on Table 5.2. Figure 5.4 shows how E_b changes as a function of cluster size.

The x axis implies the cluster size change from one atom to the "bulk" limit. 0 means bulk limit and 1 means one atom. Y axis shows the calculated E_b at each cluster size. The graph shows a very interesting result. Sn has two different crystal structures in the bulk states. One is alpha-tin, also known as gray tin. It has a diamond-like crystal structure, is stable below 13.0 C and has non metallic properties. Another is beta-tin, also known as white tin. It has a tetragonal structure, is stable above the room temperature and has metallic properties. The binding energy of bulk alpha tin was used because it has similar property as Silicon and Germanium so that it is easier to compare against it.

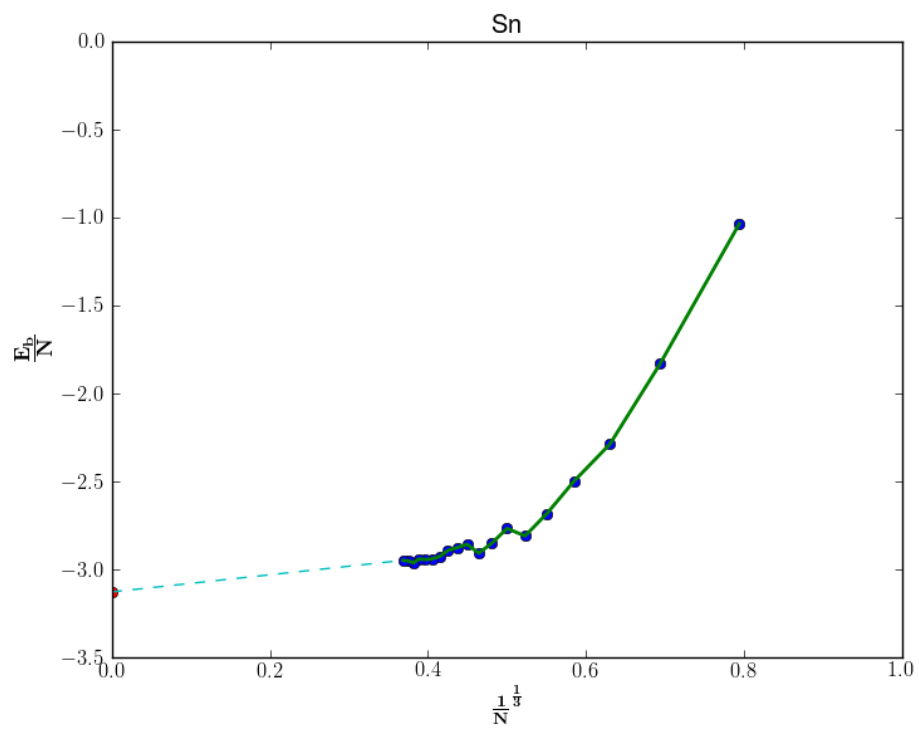


Figure 5.4: Binding energy of small Sn clusters.

The cohesive energy of Sn bulk is -3.13 eV, which was calculated by Dmol. The cohesive energy of tin bulk state is pointed at 0 on the x-axis. From size 2 to 7, the binding energy dramatically evolves and rapidly approaches the bulk limit. This indicates that those clusters have metallic bonds. Moreover, Sn clusters have different properties up to approximately 7 atoms and have bulk properties above size it. Above 7 atoms, energy changes are very smooth. To get to the bulk limit, one needs an infinite number of Sn atoms. The dash line is a prediction of how Sn clusters should evolve after size 20 (see Figure 5.4).

5.4.2 HOMO-LUMO Gap

During the relaxation process using Dmol, the HOMO-LUMO gap (which is analogous to the band gap for bulk system) is calculated by subtracting the LUMO from HOMO. The HOMO-LUMO gap of Sn clusters are shown on Table 5.2. For an easier comparison, HOMO-LUMO gaps as a function of Sn cluster sizes are plotted in Figure 5.5.

One interesting feature in the graph is that cluster size 10, the HOMO-LUMO gap is much larger compared to the other Sn clusters. Larger HOMO-LUMO gaps indicate higher stability. Sn₁₀ is, in this case, a magic number and perfect jellium model cluster with an electronic shell closing at 40 electrons. The HOMO-LUMO gap of Sn₁₀ is 1.77 eV, which makes it a good semiconductor.

5.4.3 Negatively Charged Sn Clusters

Negatively charged Sn clusters up to 20 atoms were tested with BH. Most of the structures are the same as neutral Sn clusters. However, Sn clusters at 8, 9, 10, 12, 14, 15 atom sizes have different ground state structures than neutral states. Structures are shown in Figure 5.6.

Furthermore, Vertical Electron Affinity between experimental values and the-

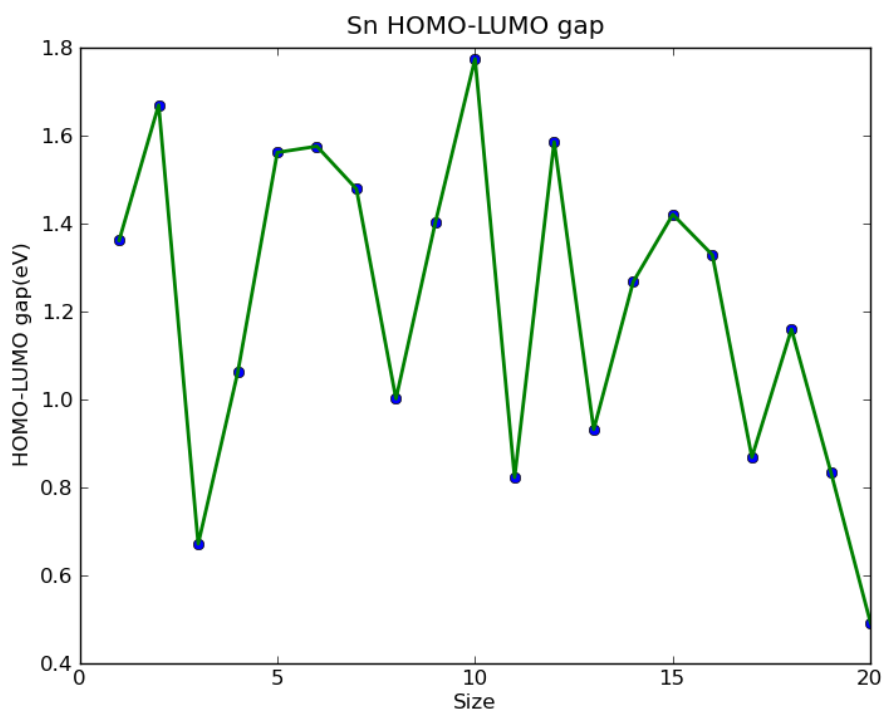


Figure 5.5: HOMO-LUMO gap of Sn clusters of 1-20 atoms.

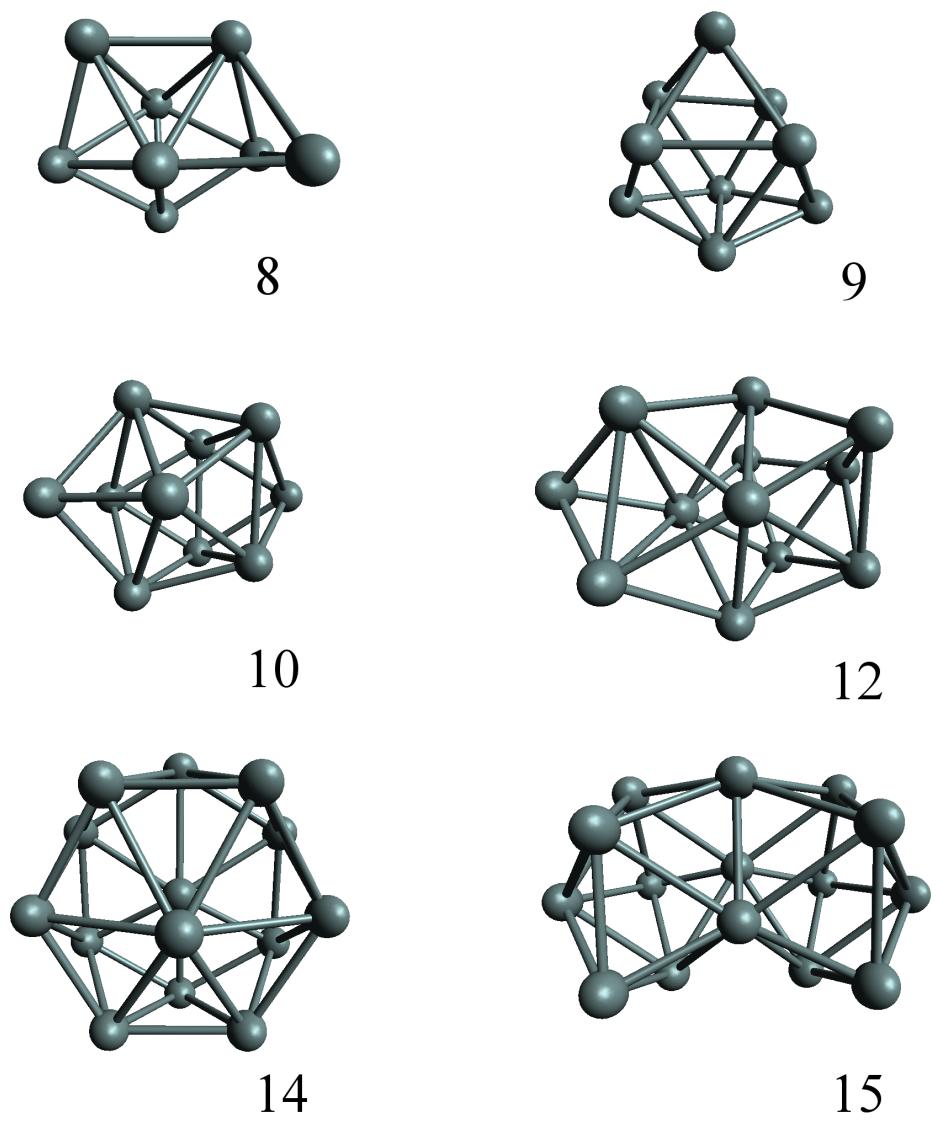


Figure 5.6: Structures of anionic Sn clusters which are found to have different structures compared to neutral ones.

oretical results are compared (see Figure 5.7). Experimental data was acquired from the work by Morave et al., [32], while VEA was calculated according to the Equation (2.8).

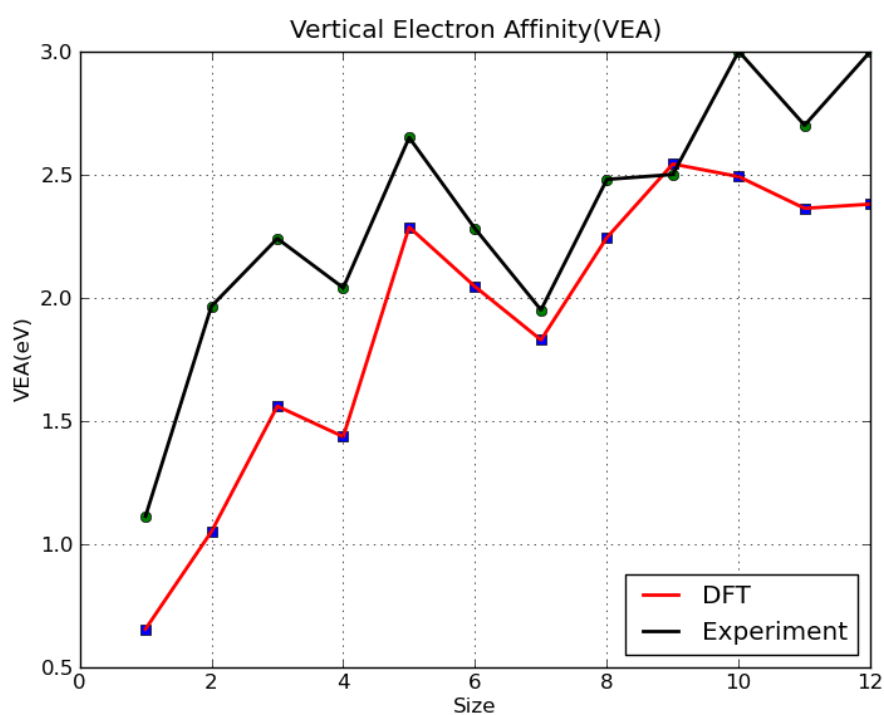


Figure 5.7: Comparison of experimental and theoretical vertical electron affinity of Sn clusters. Experimental values are taken from [32].

Chapter 6

Ru Clusters

After successfully finding the global minima of Sn, ruthenium clusters were also tested. Ruthenium is a very tricky cluster because of its many closed lying spin states. Ruthenium has an open d-shell (d^7s^1) which means that it could have high spin states or low spin states. Because of many spin states, energy convergence is a main issue. After all, global minima of Ru clusters up to 12 atoms are successfully found by the BH code. The articles by Anguilera-Granja et al. and Shetty et al. are used in order to compare the Ru clusters [33] [34].

6.1 Basin-Hopping Ru Clusters

Since the BH code deals with single elements, the “shake“ move strategy was applied. Occupation was first set to 'thermal 0.008' because the value was the most efficient for the Sn clusters. However, total energies did not converge at all. Therefore, occupation values were increased until total energies start to converge. As a results, occupation:'thermal 0.03' came as the appropriate value. Even though it is a very high value (and though the results are not completely trusted), it was the only possible value that worked for the BH code. Another important parameter is spin polarization. As mentioned earlier, Ru has a spin state since it has (d^7s^1) orbital. Therefore,different spin states have to be considered during the relaxation. Calculations were carried out using a ”coarse“ integration grid for faster calculation time. Below are the input parameters that were used for

Ru clusters:

- Spin polarization: unrestricted
- Basis: min
- Integration grid: coarse
- Functional: pbe
- Occupation: thermal 0.03

BH successfully found the local minimum and its structures for each step. However, the lowest energy structures from each cluster size are completely different compared to those reported in [33]. For example, Ru_8 has an identical structure which is a complete cube. The lowest energy structure found by BH is a complete dodecahedron. Both of the structures were relaxed with the same input parameters to confirm which of the structures have the lowest energy. The cubic structure was found to have a lower energy than dodecahedron. This was expected, as the occupation was set too high during the BH runs. However, it is impossible to lower the occupation values because the BH will not be able to run. Therefore, the only solution was to pick approximately 10 local minima Ru structures, in order to explore different atomic configurations up to 12 atoms size.

6.2 Relax the Selected Structures from Basin-Hopping Results

Approximately 10 local minima structures were picked from the BH results. They were relaxed with the input parameters that were used in re-relaxation of Sn clusters. During the re-relaxation process, the values of occupation were decreased slowly. It took approximately 10 relaxations before they can be relaxed with occupation 'Fermi'. As was expected, the lowest energy structures from BH are not the lowest energy ones. After going through every single relaxed structure, the lowest energy structures were successfully found to be the same as references

[33], [34]. Figure 6.1 shows the corresponding global minima Ru structures that were found with BH.

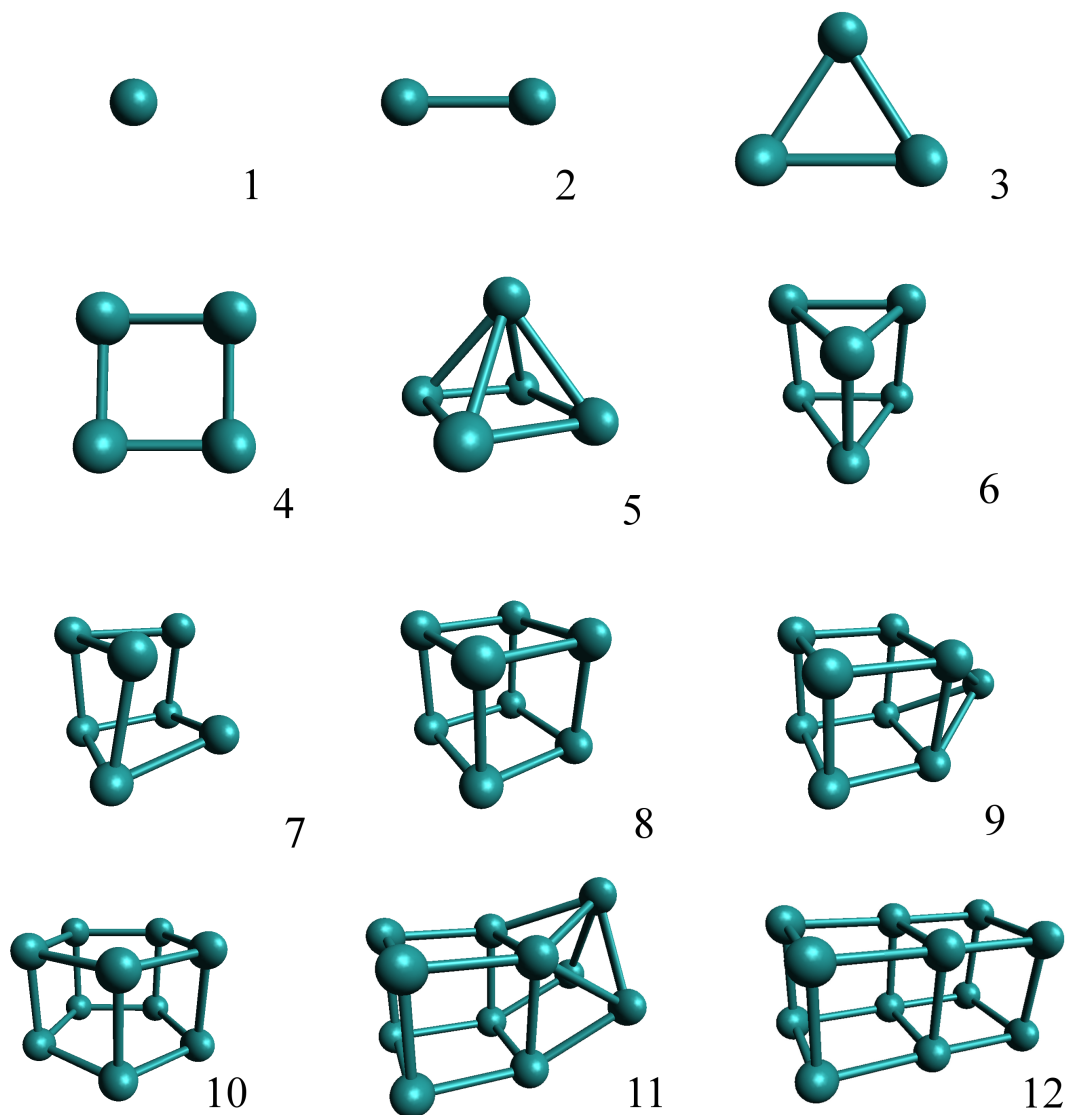


Figure 6.1: Ground States Structures for Ru_1 - Ru_{12} clusters.

Figure 6.1 shows that Ru clusters tend to form cubic-like structures.

6.3 Energetic Analysis

6.3.1 Binding Energy

Binding energy of Ru was calculated by Equation (2.3). Table 6.1 shows binding energy at each cluster size. Evolution of E_b as a function of Ru cluster size is plotted in Figure 6.2.

Size	E_b (eV)	HOMO-LUMO Gap(eV)	Mean Distance \AA
1	0.00000	0.921	0.0000
2	-4.18646	0.582	2.1696
3	-8.51990	0.512	2.3954
4	-12.90218	0.360	2.3141
5	-18.47746	0.693	2.4432
6	-23.28891	0.231	2.4052
7	-28.55767	0.032	2.4484
8	-34.87034	0.050	2.3753
9	-39.06253	0.099	2.4672
10	-43.99072	0.462	2.3699
11	-49.11250	0.169	2.4626
12	-55.56250	0.555	2.4057

Table 6.1: Binding energy, HOMO-LUMO gap and mean distances.

Binding energy of Ru bulk was also calculated by using Dmol. It has -7.06 eV, which is pointed at 0 on the x-axis. Compared to Sn clusters, Ru have a rather smooth straight line evolution of E_b as a function of size.

6.3.2 HOMO-LUMO Gap and Magnetic Properties

Ru has smaller HOMO-LUMO gap than Sn does. From Figure 6.3, it can be noticed that sizes 7,8 and 9 atoms have a particularly small HOMO-LUMO gap.

Bulk Ru behaves paramagnetic because of its unpaired electron. However, some small Ru clusters behave non-magnetic. Table 6.2 shows that Ru clusters

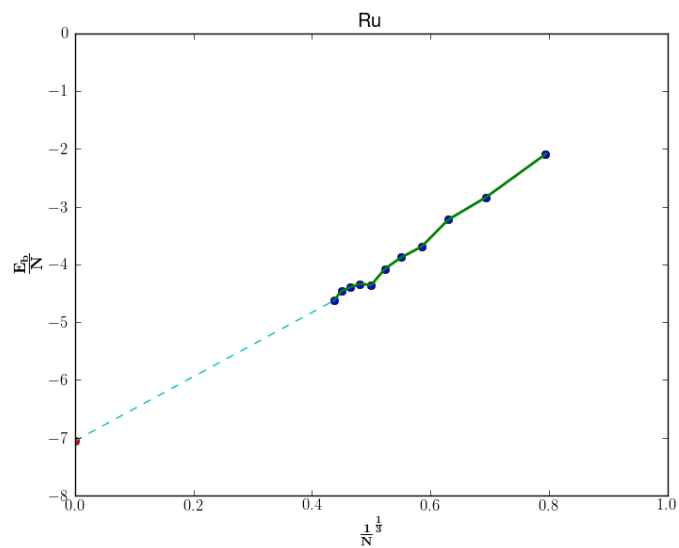


Figure 6.2: Binding energy for Ru clusters.

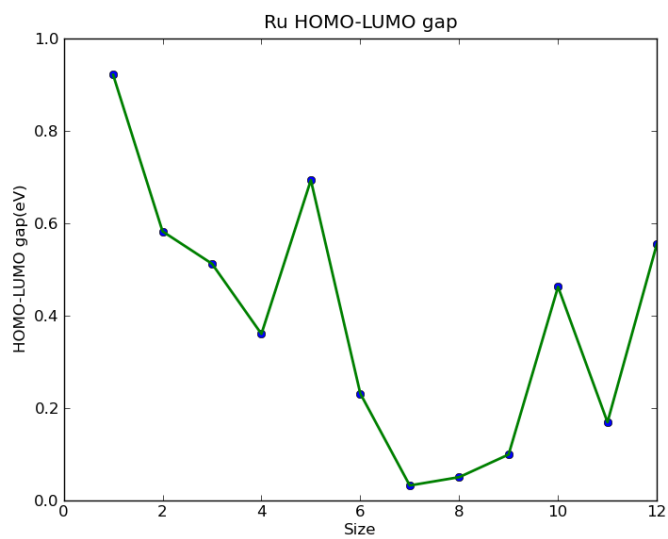


Figure 6.3: HOMO-LUMO gap of Ru clusters of 1-20 atoms.

at sizes 5,10 and 12 atoms have no unpaired electrons. It is interesting that a magnetic material in the bulk state can be nonmagnetic in some of their small clusters.

Size	Unpaired Electron	Magnetism
1	6	Paramagnetic
2	4	Paramagnetic
3	6	Paramagnetic
4	2	Paramagnetic
5	0	Diamagnetic
6	2	Paramagnetic
7	2	Paramagnetic
8	4	Paramagnetic
9	8	Paramagnetic
10	0	Diamagnetic
11	2	Paramagnetic
12	0	Diamagnetic

Table 6.2: Magnetic properties of Ru clusters.

Chapter 7

Ru-Sn Clusters

Bimetallic clusters Ru_xSn_y are tested in this chapter. For ease of analysis and comparison with single Ru and Sn clusters, the values of x and y were made equivalent to each other (i.e. 50-50% composition).

7.1 Basin-Hopping, Ru-Sn

Global optimization of Ruthenium Tin (Ru-Sn) clusters are now performed with the BH code. The BH code had to be modified for this binary system. “Swap every 10 hybrid“ move was used as a move strategy. Dmol input parameters are listed below:

- Spin polarization: unrestricted
- Basis: dn
- Integration grid: medium
- Functional: pbe
- Occupation: thermal 0.01

7.2 Relax the Selected Structures from Basin-Hopping Results

Approximately 5 structures were chosen from the BH results. Those Ru-Sn structures were all relaxed with input parameters which were also used for Ru and Sn clusters. Figure 7.1 shows the ground states structures of Ru-Sn up to size $x+y=16$.

7.3 Structure Analysis

Figure 7.1 shows some interesting features. Ru tends to stay together (occupying core positions) and Sn clusters cap to Ru. One explanation of this is that Ru has larger surface energy than Sn.

Figure 7.2 and Table 7.1 shows the mean distance of Ru-Sn, Ru-Ru and Sn-Sn in the Ru-Sn cluster. It has to be noted that there are not any Sn-Sn bonds in Ru_5Sn_5 . The graph indicates that Ru has strong bonds with Ru and Sn.

7.4 Energetic Analysis

7.4.1 Binding Energy

The binding energy of Ru-Sn clusters were calculated by Equation (2.5). Table 7.1 shows the Binding energy of Ru-Sn clusters. Binding energy of Ru_5Sn_5 has a particularly large value. The rest of the clusters behave more linearly by increasing the cluster size. Therefore, Ru_5Sn_5 could be said magic number clusters because of its high stability.

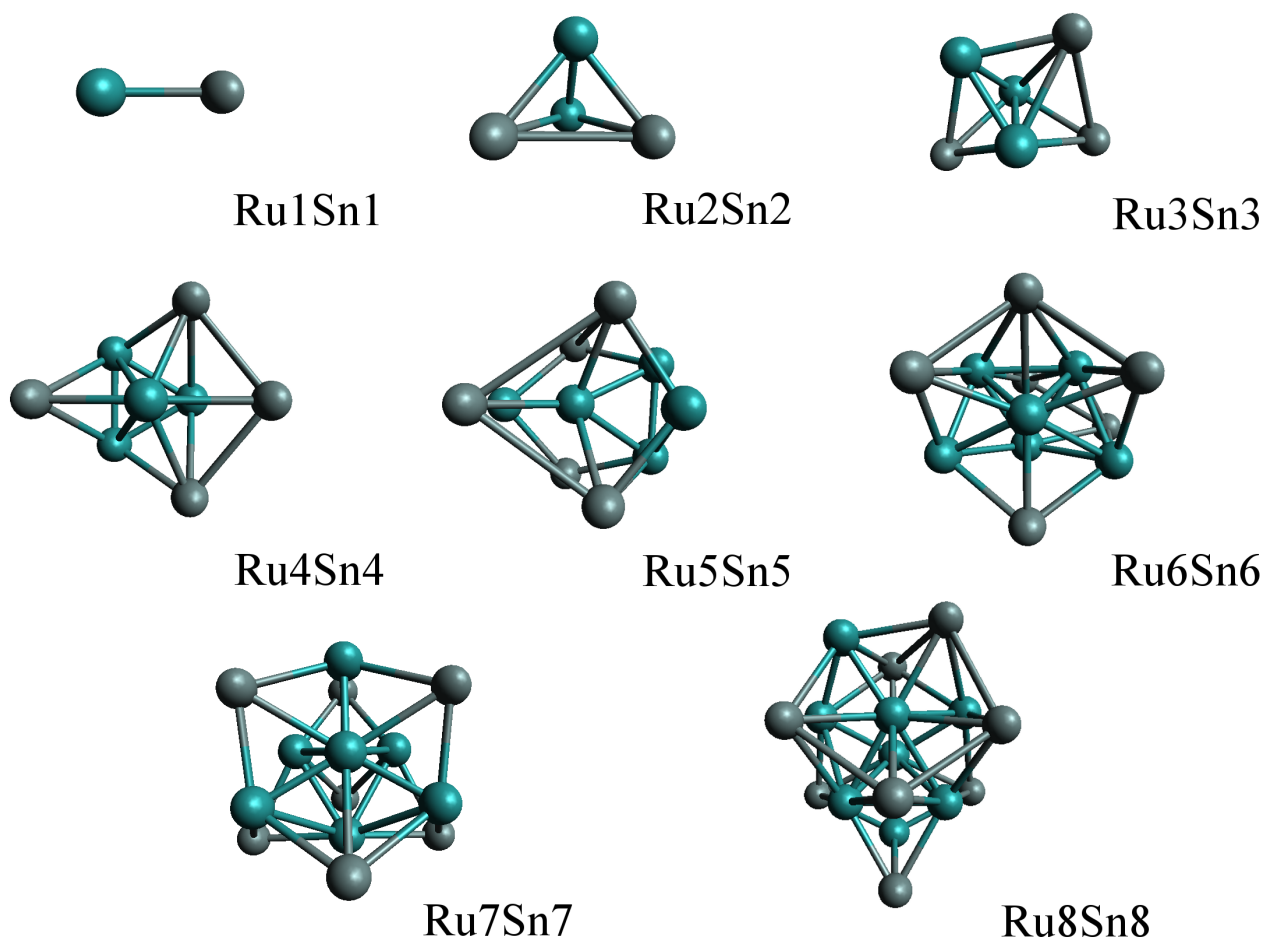


Figure 7.1: Ground state structures of Ru_XSn_Y , $X+Y \leq 16$.

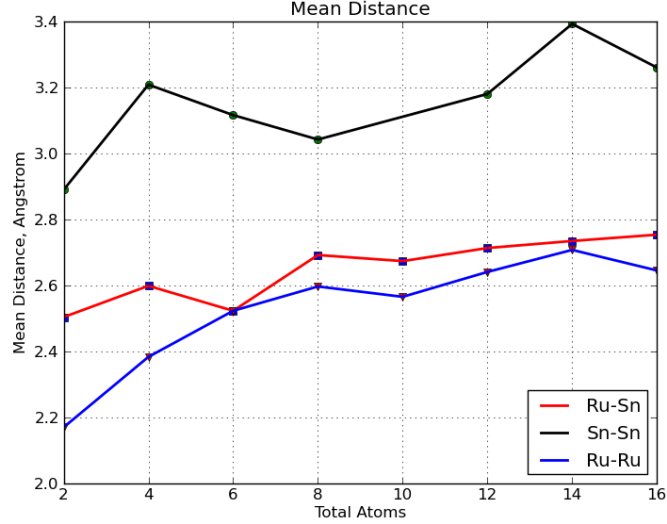


Figure 7.2: Mean distance in Ru-Sn clusters.

Ru_XSn_Y	E_b (eV)	H-L gap(eV)	Ru-Sn(Å)	Ru-Ru(Å)	Sn-Sn(Å)
11	-3.81904	0.778	2.5035	None	None
22	-5.88108	0.697	2.5983	2.3830	3.2079
33	-6.38230	0.886	2.5227	2.5227	3.1156
44	-6.95585	0.374	2.6916	2.5963	3.0417
55	-6.55546	0.403	2.6732	2.5650	None
66	-8.25574	0.202	2.7128	2.6404	3.1798
77	-8.91014	0.377	2.7342	2.7071	3.3922
88	-9.09476	0.294	2.7533	2.6449	3.2598

Table 7.1: Binding energy, H-L gap and Mean distance.

7.4.2 HOMO-LUMO Gap

The HOMO-LUMO gap of Ru-Sn is listed and plotted in Table 7.1 and Figure 7.3. It has to be noted that total size of Ru-Sn corresponds to the number of Ru and Sn Atoms in Figure 7.3. Figure 7.3 also indicates that the HOMO-LUMO gap of Ru-Sn clusters is located somewhere between Sn and Ru clusters.

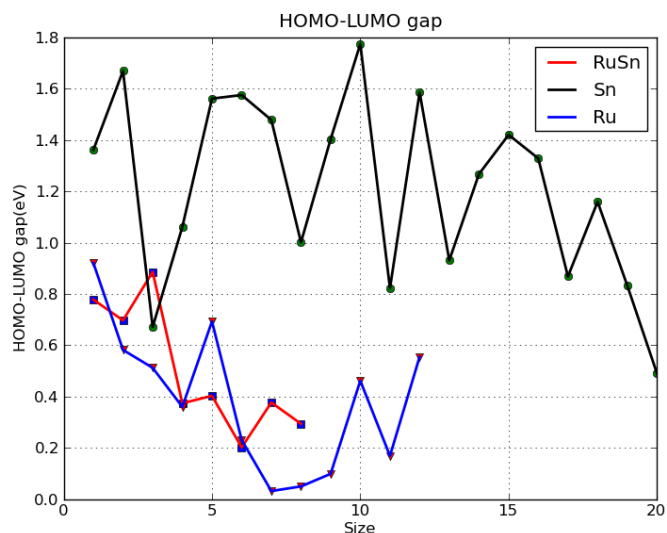


Figure 7.3: HOMO-LUMO gap for Ru-Sn clusters.

7.5 Ru-Sn Clusters Supported on SiO₂

So far, all cluster structures have been studied in the gas phase. However, clusters are generally grown on insulating surface such as silicon dioxide. For this project, the (001) face of α -cristobalite was used as the surface. Therefore, it is interesting to see if clusters supported on an oxide surface have the same structural arrangements compared to those in the gas phase.

For this, the BH code had to be modified to include the oxide surface, i.e. 2 layers of an SiO₂ surface had to be created during the BH process so that only the top layer of the surface was relaxed along with the clusters. Then, only the clusters added to the surface are "shaken" and "swapped" during the BH process. Throughout the whole process, the surface remains unchanged.

With the modified code, the BH code was run for 500 steps. Figures 7.4, 7.5, 7.6 show the ground state structure of Ru-Sn clusters on the SiO₂ surface. One

interesting thing to notice is that the ground state structures of supported Ru-Sn clusters differ from their gas phase counterparts. Therefore, it is shown that Ru-Sn cluster structures are directly affected by the oxide-surface where they are supported.

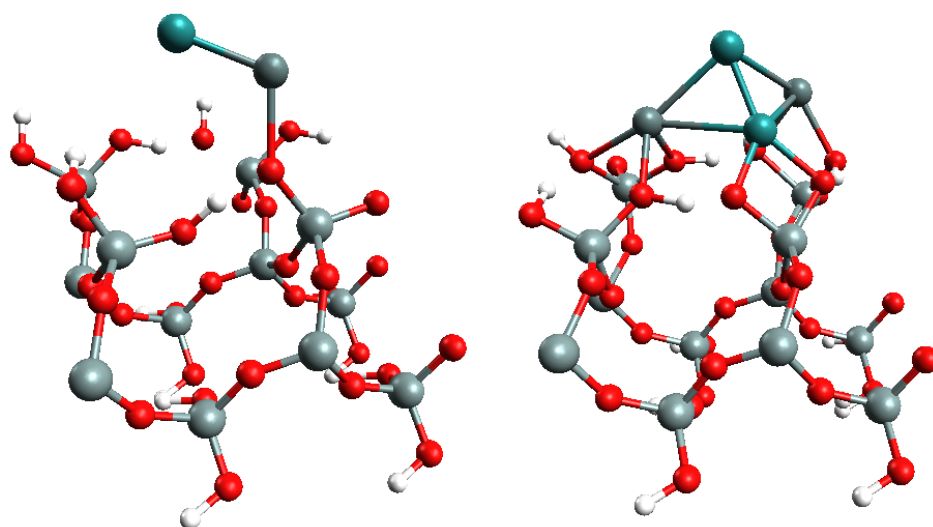


Figure 7.4: Ground States structures of $\text{Ru}_1\text{Sn}_1, \text{Ru}_2\text{Sn}_2$ on SiO_2 surface.

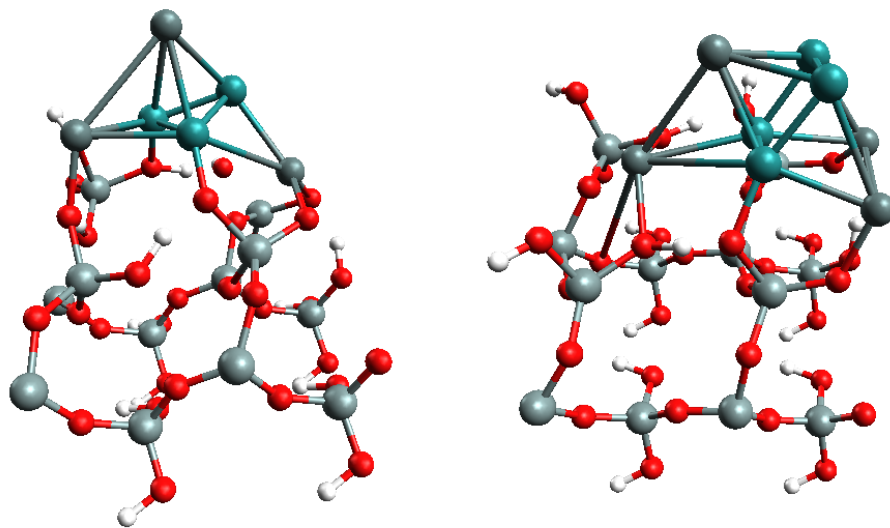


Figure 7.5: Ground States structures of $\text{Ru}_3\text{Sn}_3, \text{Ru}_4\text{Sn}_4$ on SiO_2 surface.

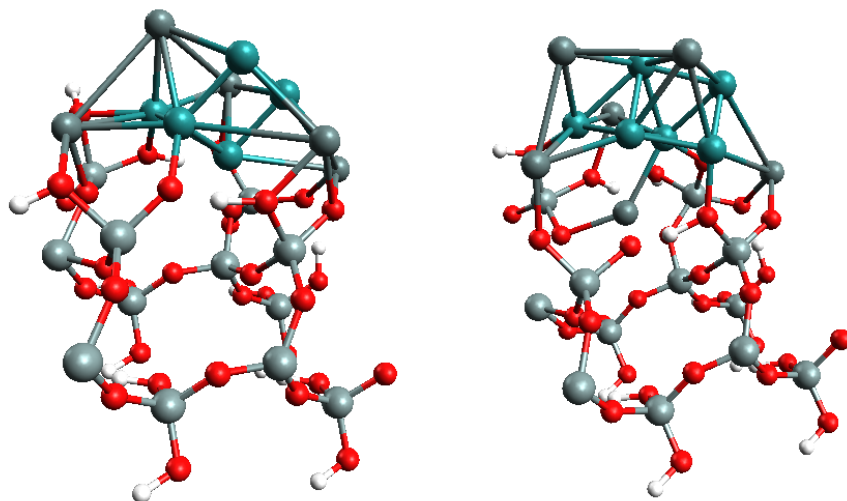


Figure 7.6: Ground States structures of $\text{Ru}_5\text{Sn}_5, \text{Ru}_6\text{Sn}_6$ on SiO_2 surface.

Chapter 8

Basin-Hopping with Hydrogen Atom

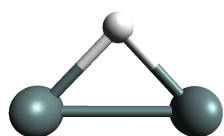
It has been noted that bimetallic clusters are much more efficient catalysts than pure element clusters. However, the reason for that is still remains unknown. In order to understand the reason, one hydrogen atom was chemisorbed to Ru,Sn and Ru-Sn clusters. Those cluster configurations involving 1 H atom were optimized using the BH code.

8.1 Sn Clusters with Hydrogen

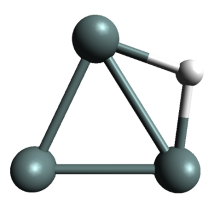
Global optimizations of Sn clusters up to size 6 atoms, involving one hydrogen atom, were analyzed with the BH code. Figure 8.1 shows the ground state structures of Sn clusters with chemisorbed hydrogen. From these structures, it is quite hard to find a bonding trend, but one could say that hydrogen is always attached at the surface of Sn clusters at both top and bridge positions.



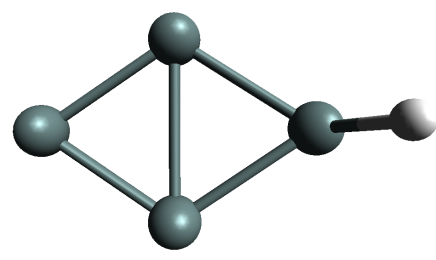
SnH



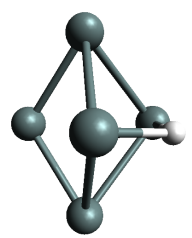
Sn2H



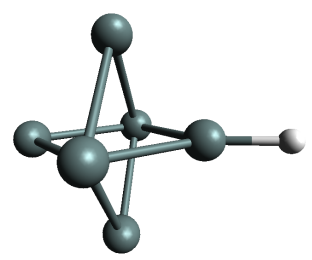
Sn3H



Sn4H



Sn5H



Sn6H

Figure 8.1: Ground state Sn clusters(1-6 atoms) with 1 chemisorption hydrogen atom.

8.2 Ru Clusters with Hydrogen

Global optimizations were also performed for Ru clusters involving one hydrogen atom. Figure 8.2 shows the ground state structures of Ru clusters with 1 chemisorbed hydrogen atom. After comparing the Ru and Sn cluster with hydrogen, a feature was found. Ru_4 and Sn_4 are both planar structures. For these two clusters, the hydrogen atom is bound to one element only, in a top position. However, hydrogen bonds with two atoms in the bridge position when the clusters are three dimensional (with the exception of Sn_6H and Ru_5H).

8.3 Ru-Sn Clusters with Hydrogen

Global optimization of Ru-Sn clusters with one hydrogen atom was performed using the BH code. Figure 8.3 shows the ground state structure of Ru-Sn clusters with 1 chemisorbed hydrogen atom. One of the interesting features is that the hydrogen atom is always found to be bound to Ru atoms (both in top and bridge configurations).

8.4 Binding Energy of Hydrogen

The binding energy of a hydrogen atom in Ru-Sn, Ru and Sn clusters was calculated by Equations (2.6) and (2.7). Table 8.1 and Figure 8.4 shows the corresponding binding energy of a hydrogen atom for each cluster size. At sizes 4, 5 and 6 atoms in Sn clusters, the sign of the binding energy becomes positive, meaning it is endothermic. The hydrogen does not want to bond with Sn. It is interesting to note that Ru_6Sn_6 also shows endothermicity towards the hydrogen atom, i.e. the binding between a hydrogen atom and the bimetallic cluster is not favorable.

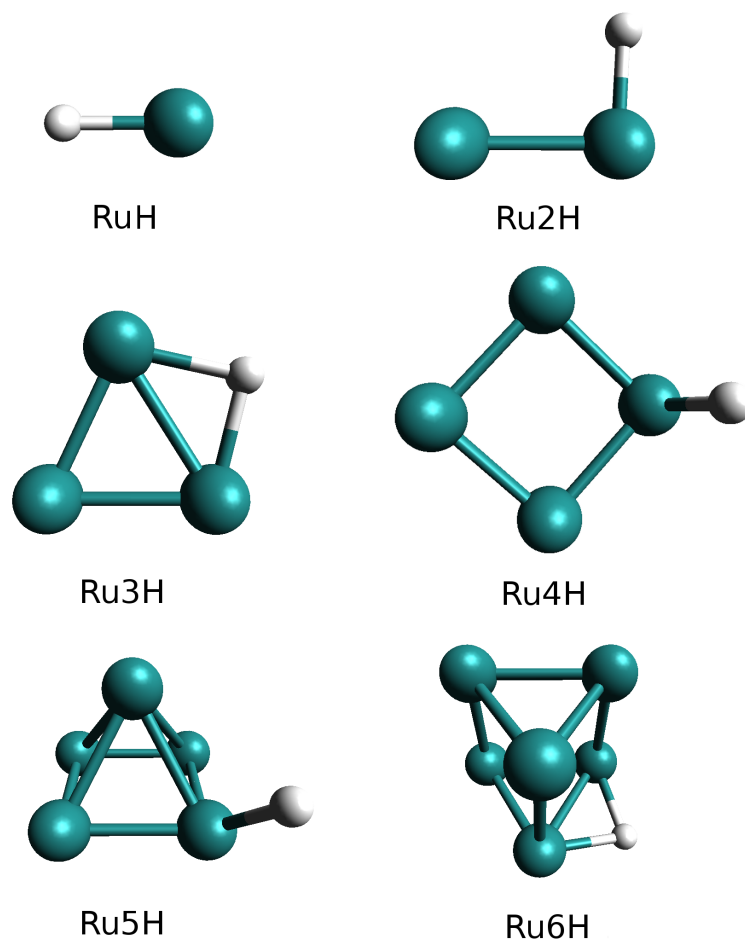


Figure 8.2: Ground state Ru clusters(1-6 atoms) with 1 chemisorption hydrogen atom.

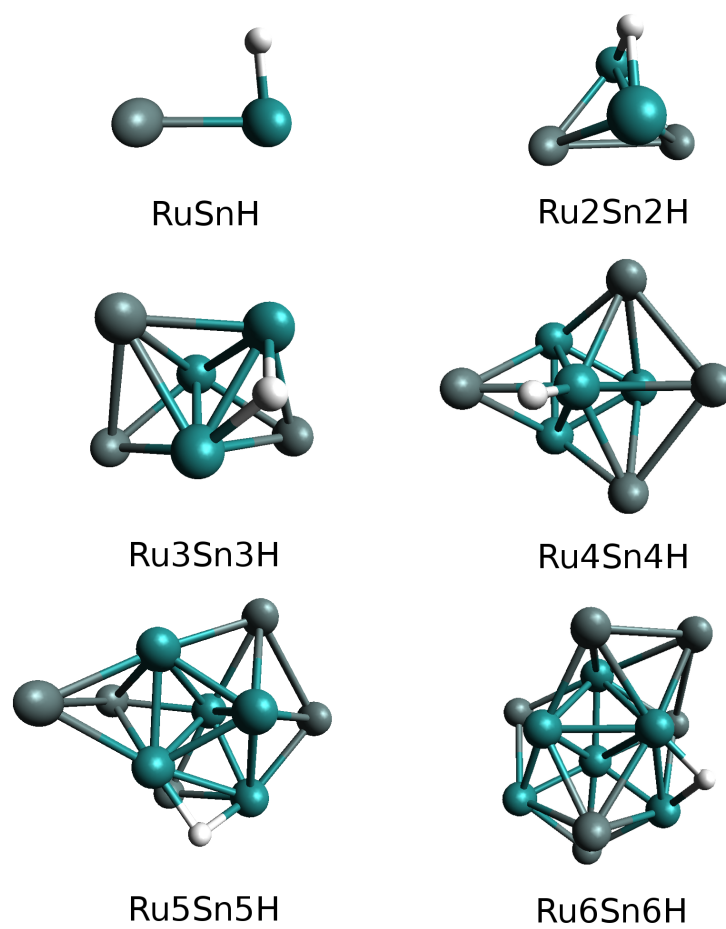


Figure 8.3: Ground state Ru-Sn clusters(1-6 atoms) with 1 chemisorption hydrogen atom.

Size	$E_b(\text{H in Sn})/(\text{eV})$	$E_b(\text{H in Ru})/(\text{eV})$	$E_b(\text{H in Ru-Sn})/(\text{eV})$
1	-0.28944	-1.27270	-0.80962
2	-0.76980	-0.29670	-0.47266
3	-0.41425	-0.61464	-0.39750
4	0.46546	-0.87973	-0.50394
5	0.20291	-0.43417	-0.99704
6	0.47567	-0.56151	0.157469

Table 8.1: Binding energy of an hydrogen atoms in each system.

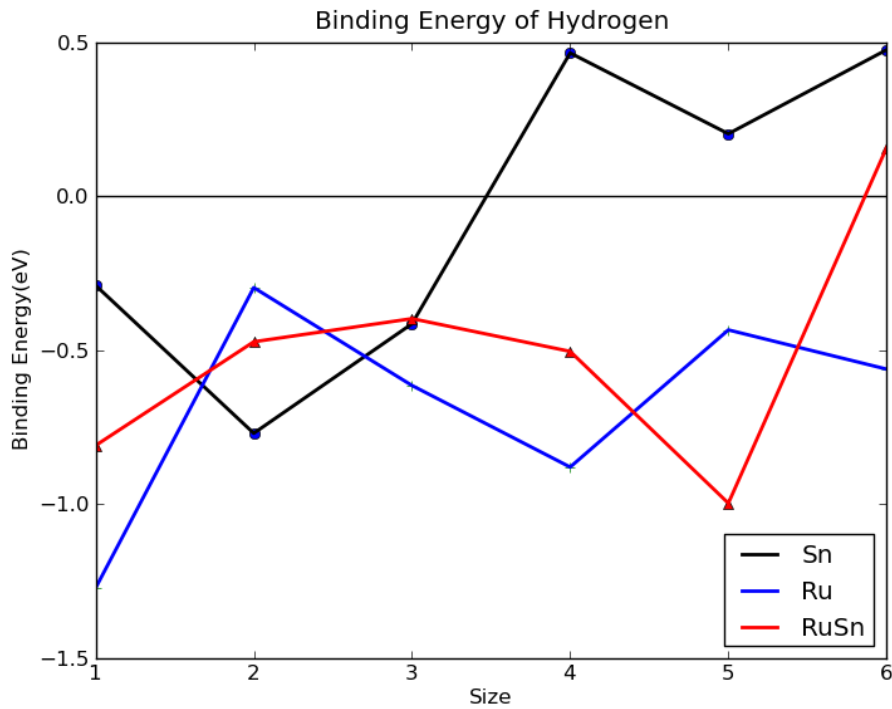


Figure 8.4: Binding energy of an hydrogen atom in each system.

Chapter 9

Conclusions

The Basin-Hopping (BH) algorithm, coupled with a DFT software (Dmol), was successfully constructed and proven to be a useful tool in determining the lowest energy structures of clusters up to 20 atoms for both of mono- and bimetallic clusters. The BH-DFT method found much more stable structures of Sn clusters up to 20 atoms than previously-reported structures. Sn₁₀ in particular had a very large HOMO-LUMO gap and its structure can be considered a magic number structure. The most interesting part of Sn cluster is the rapid evolution of binding energy towards bulk limit by increasing the cluster size. The binding energy of a Sn₈ cluster already has a similar binding energy compared to the bulk cohesive energy. The vertical energy affinity of Sn cluster, calculated by BH and DFT methods presents the same trend as the experimental results. This proves that the results with BH-DFT can be trusted. Ru clusters were very tricky because of its unstable spin states. However, BH-DFT was able to find the global minimum for each cluster size, even though the global minimum does not always initially appear as the lowest energy configuration during the initial BH-DFT runs. Therefore, approximately five different structures needed to be selected from the results to be strictly relaxed. As a result, the ground state structures of Ru clusters up to 12 atomic were successfully found. It is interesting to see that some of the small Ru clusters have non-magnetic properties, which are in contrast with the bulk metal. The ground state structures of Ru-Sn clusters up to 20 atoms were also successfully found. These clusters demonstrated that Ru tends to bond together with other Ru atoms occupying core positions and Sn attaches

to Ru like a cap (segregates to the surface). The electric properties of Ru-Sn clusters are located somehow between Sn and Ru clusters. Supported Ru-Sn clusters on SiO_2 tend to have different atomic arrangements compared to the gas-phase counterparts. Global optimization of Ru, Sn, and Ru-Sn clusters including 1 chemisorbed hydrogen atom was very difficult to analyze because there were no clear trends. However, hydrogen tends to bond with Ru within Ru-Sn clusters. Until experimental work catches up with technology, the BH-DFT global optimization method will be key to understanding the atomic structures of clusters consisting of a few tens of atoms.

Appendix A: Structures of Monometallic Clusters

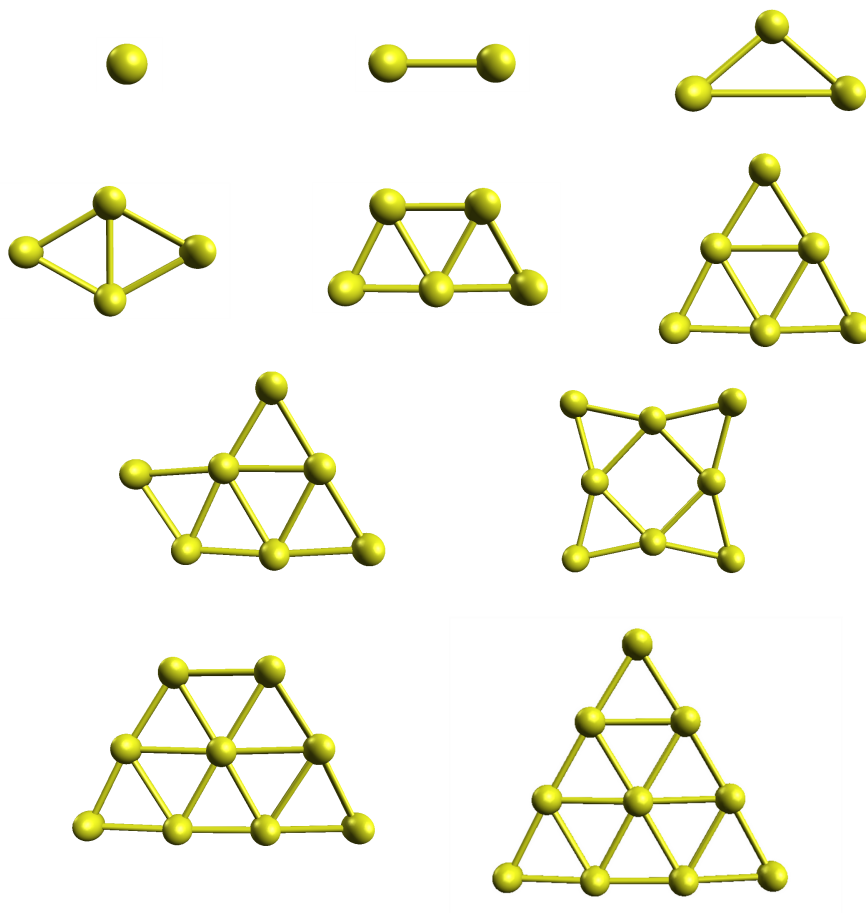


Figure 1: Ground States Structures for $Au_1 - Au_{10}$.

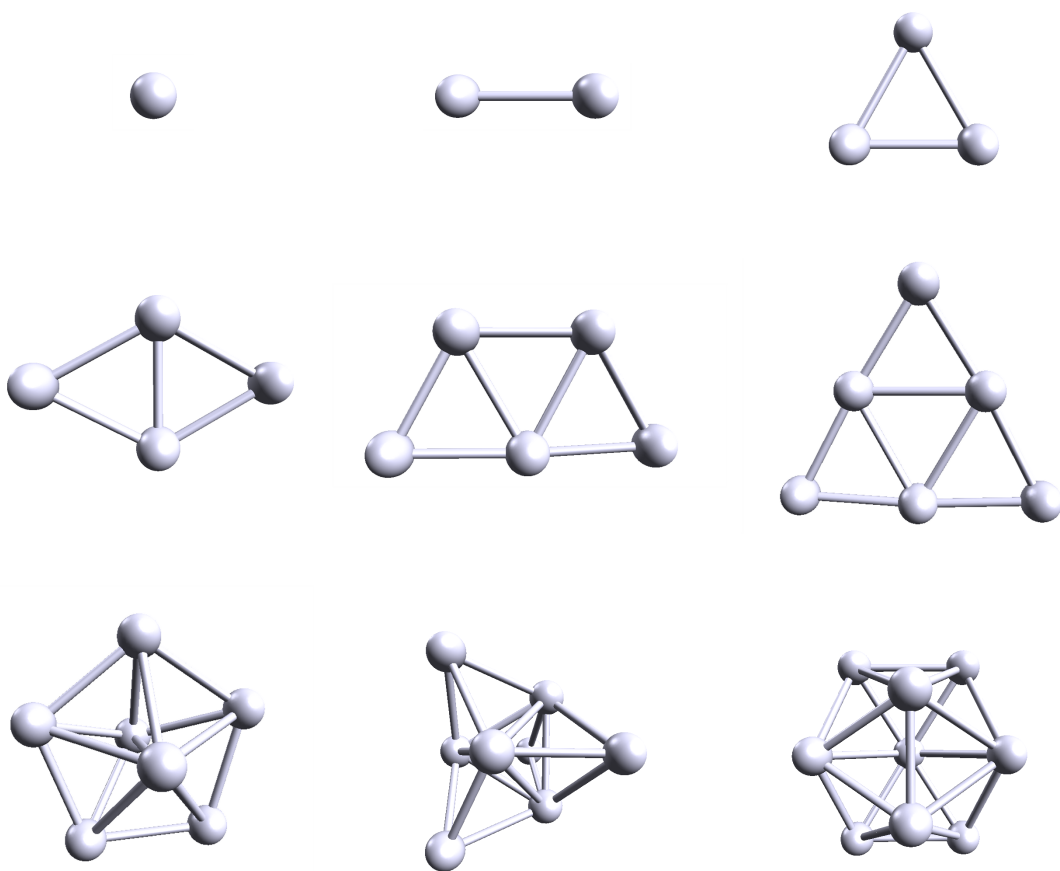


Figure 2: Ground States Structures for Ag_1 - Ag_9 .

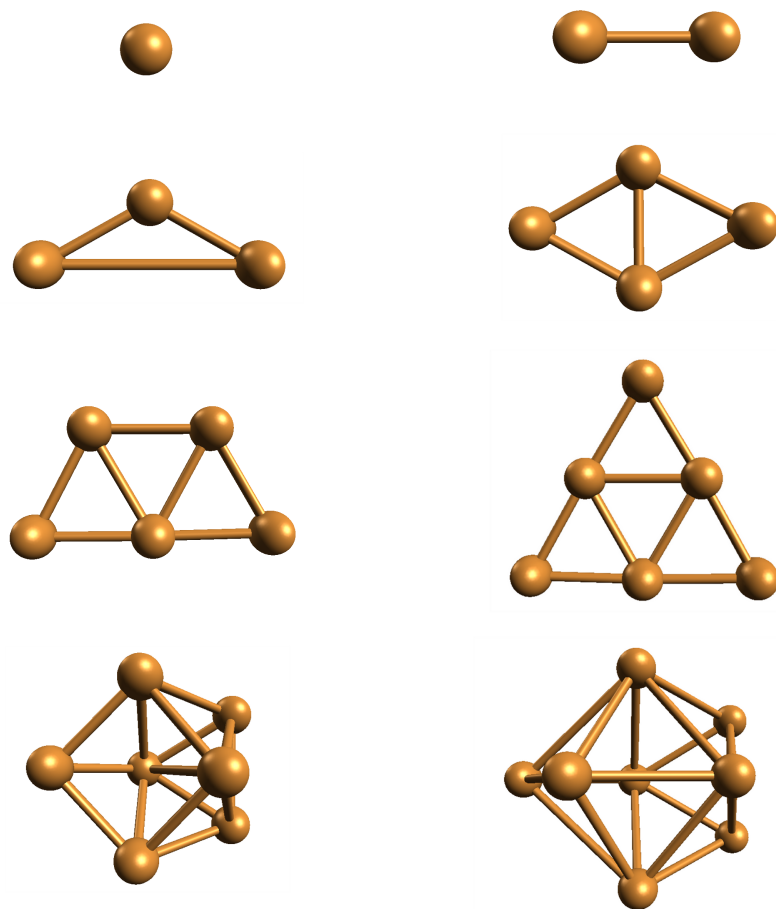


Figure 3: Ground States Structures for $\text{Cu}_1 - \text{Cu}_8$.

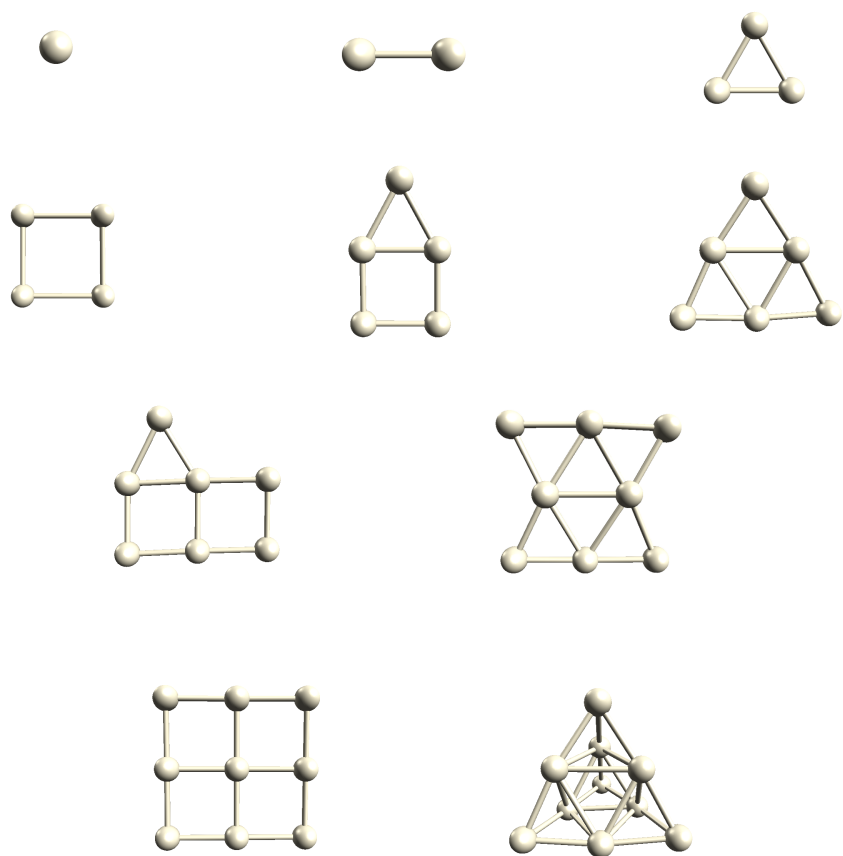


Figure 4: Ground States Structures for Pt₁ - Pt₁₀.

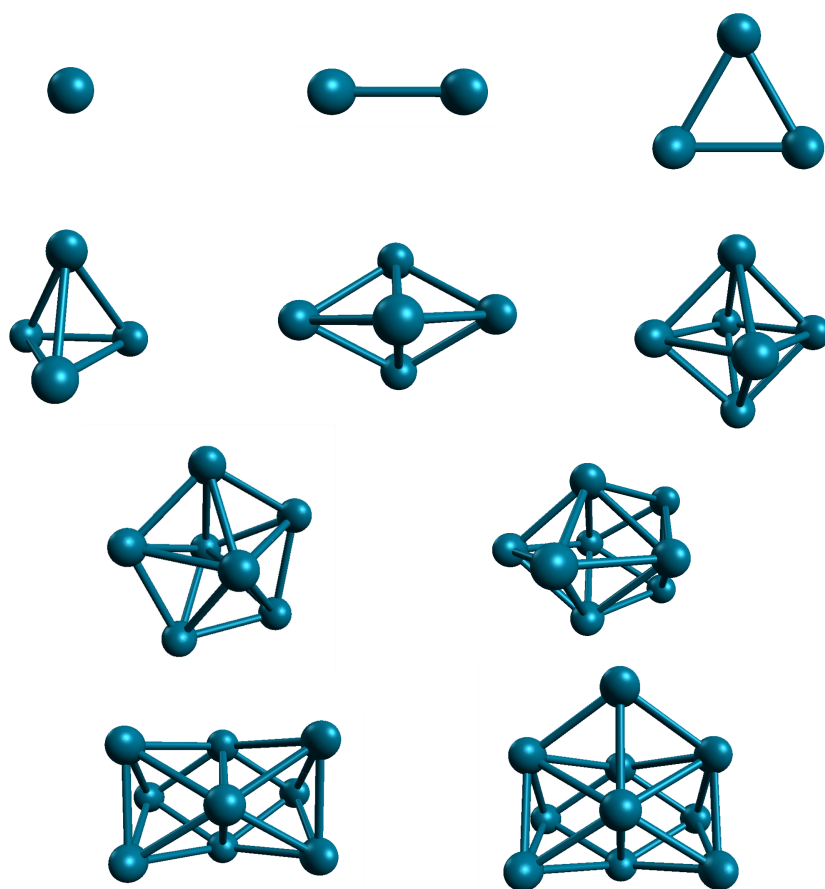


Figure 5: Ground States Structures for Pd₁ - Pd₁₀.

Appendix B: Structures of Bimetallic Clusters

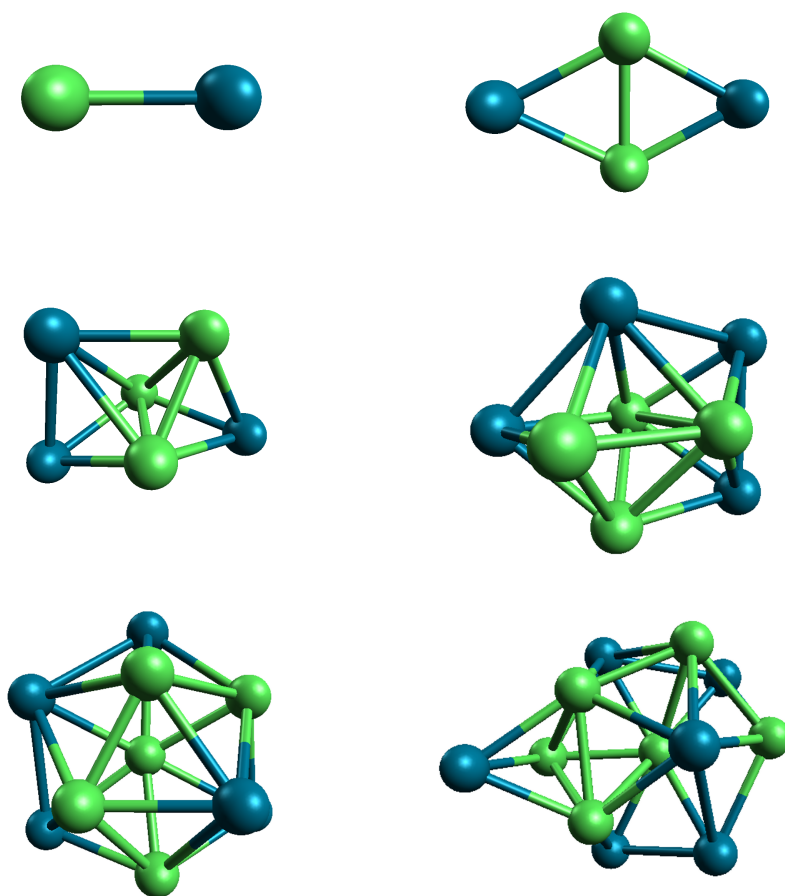


Figure 6: Ground States structures of Ni_XPd_Y , $X+Y \leq 12$.

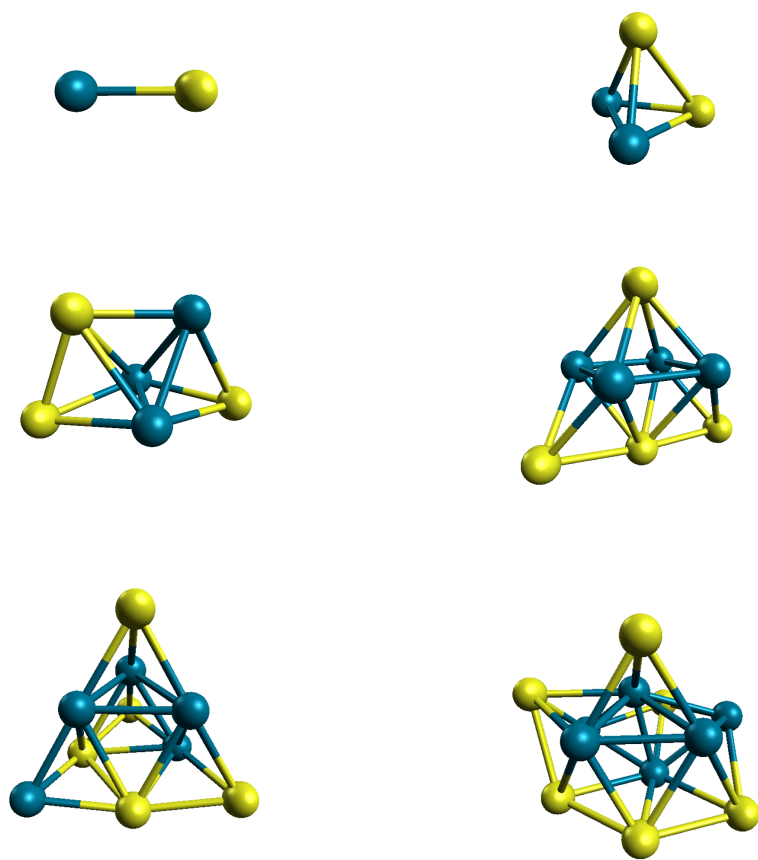


Figure 7: Ground States structures of Pd_xAu_y, X+Y≤12.

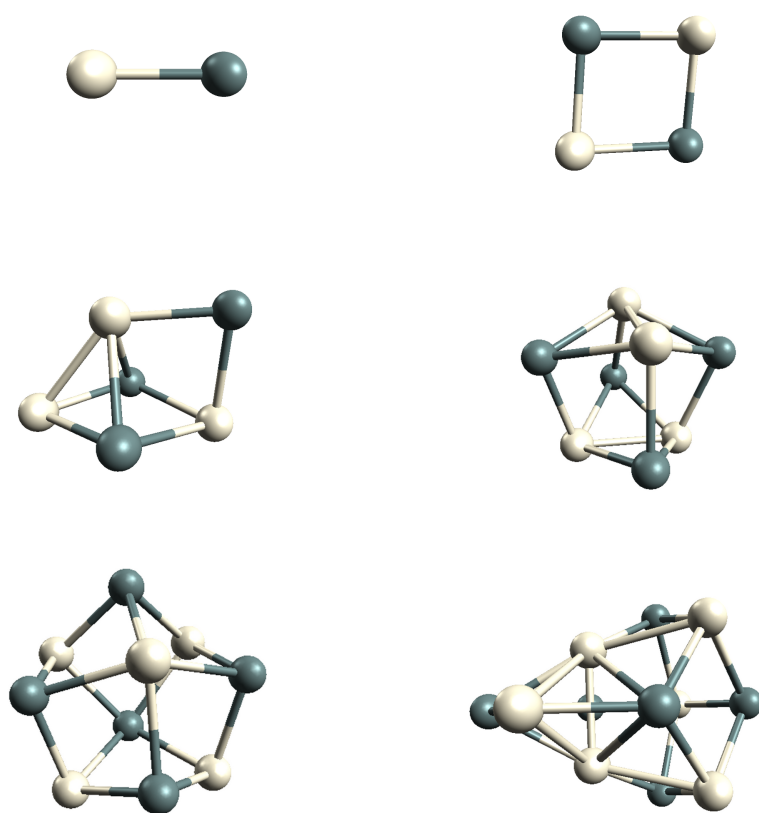


Figure 8: Ground States structures of Pt_XSn_Y , $X+Y \leq 12$.

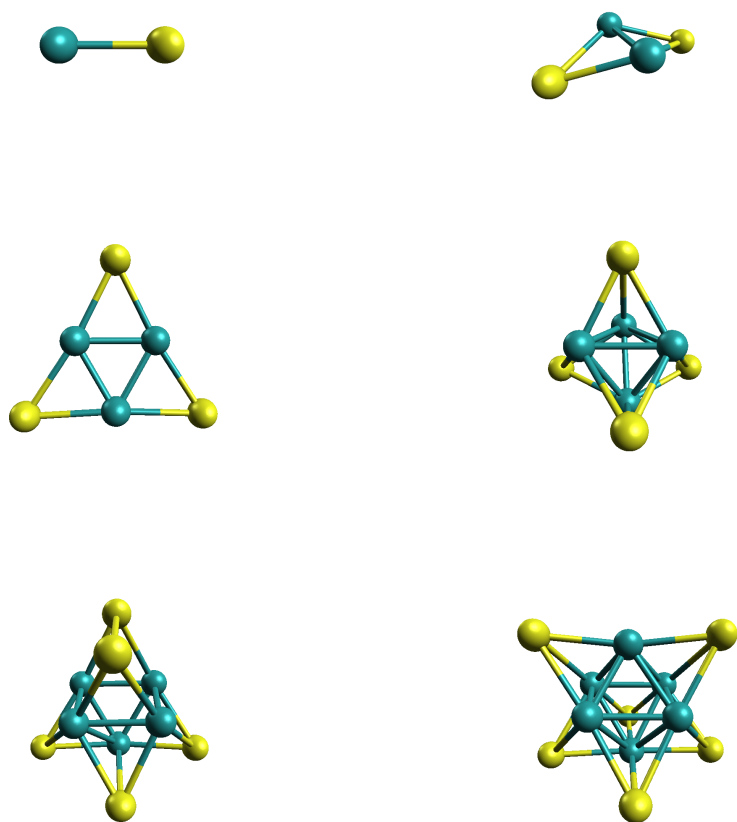


Figure 9: Ground States structures of Ru_XAu_Y , $X+Y \leq 12$.

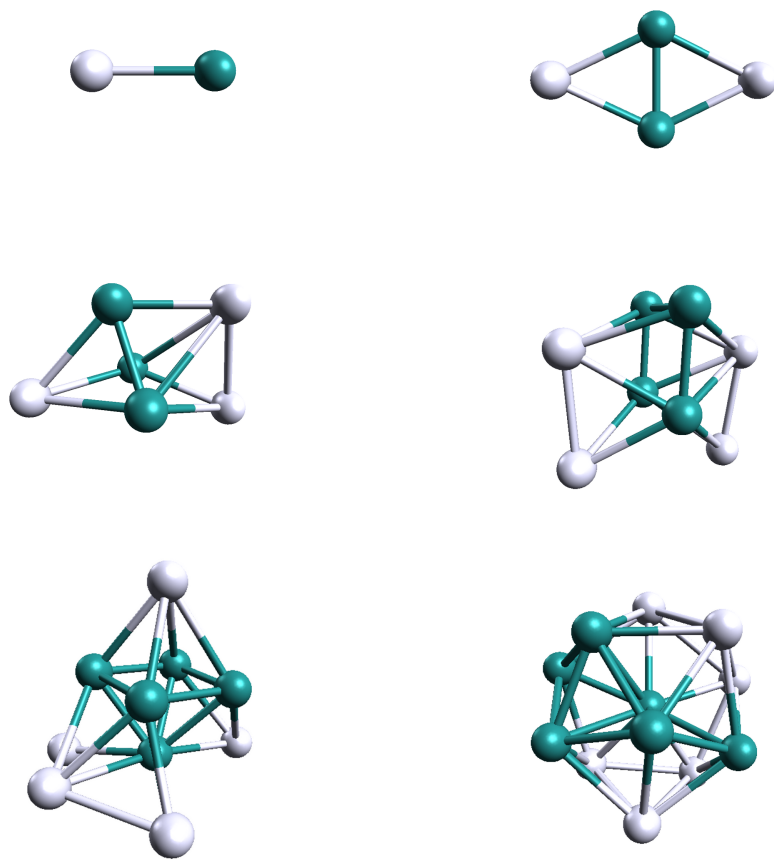


Figure 10: Ground States structures of Ru_XAg_Y , $X+Y \leq 12$.

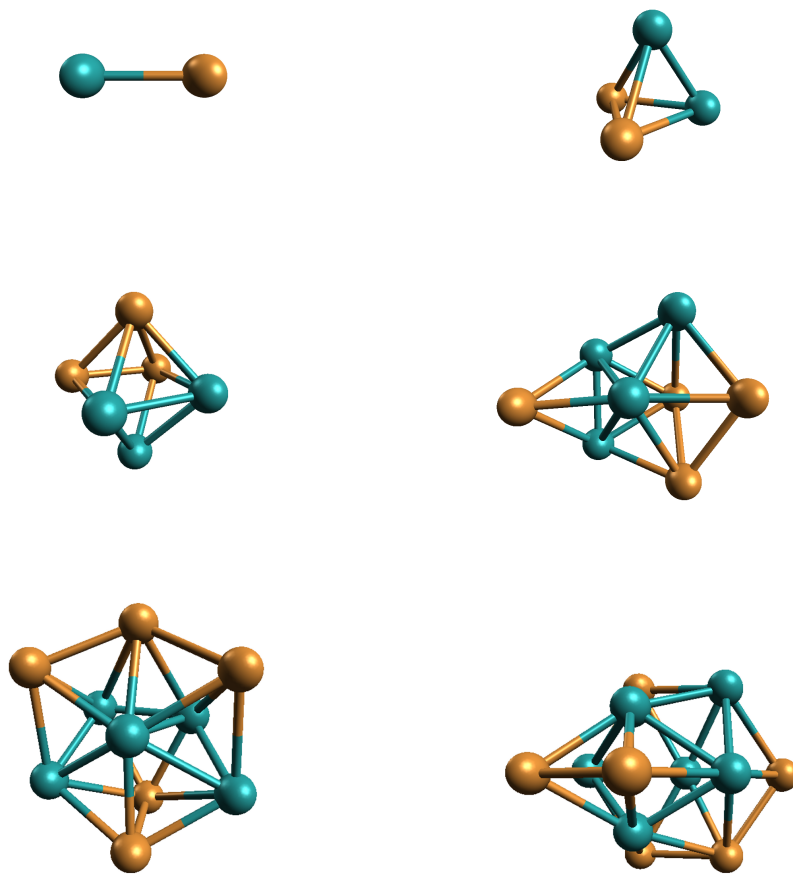


Figure 11: Ground States structures of Ru_XCu_Y , $X+Y \leq 12$.

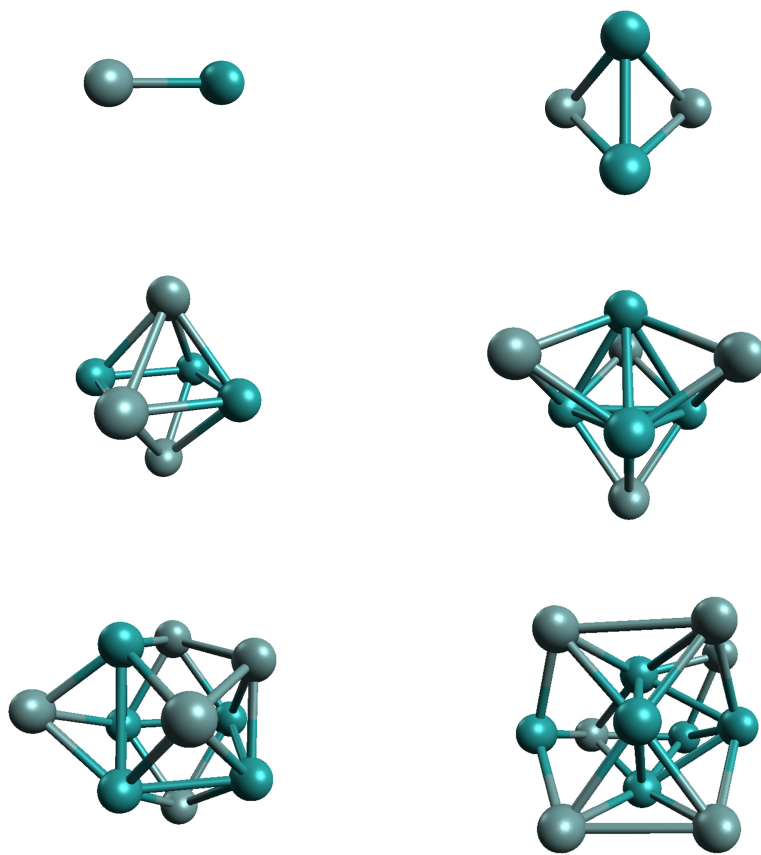


Figure 12: Ground States structures of Ru_XGe_Y , $X+Y \leq 12$.

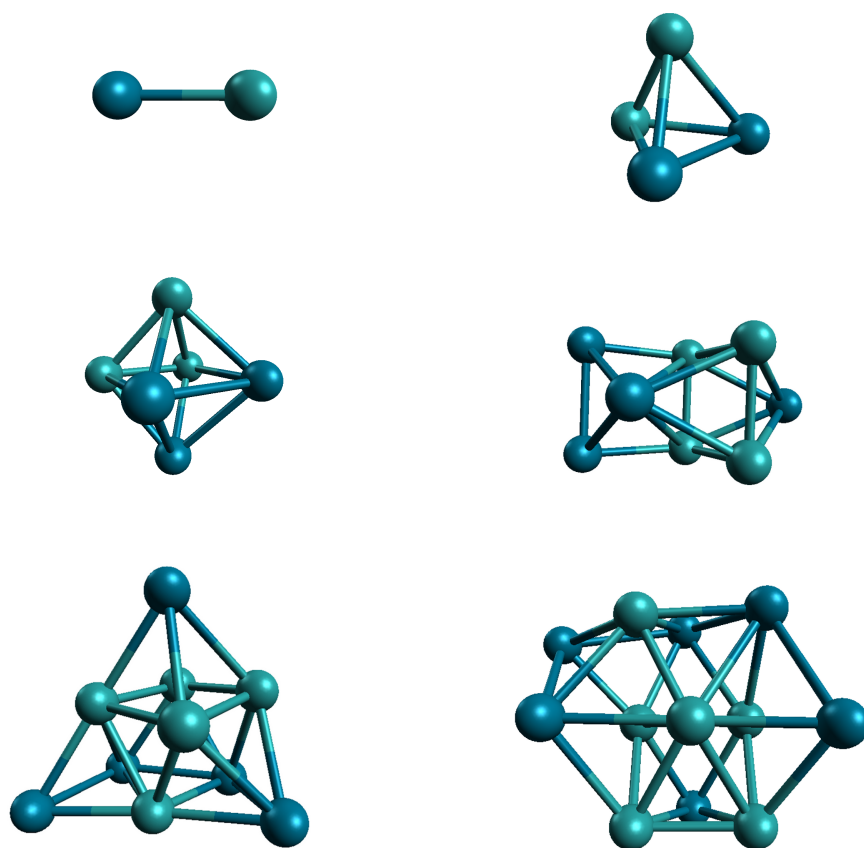


Figure 13: Ground States structures of Ru_xPd_y, X+Y≤12.

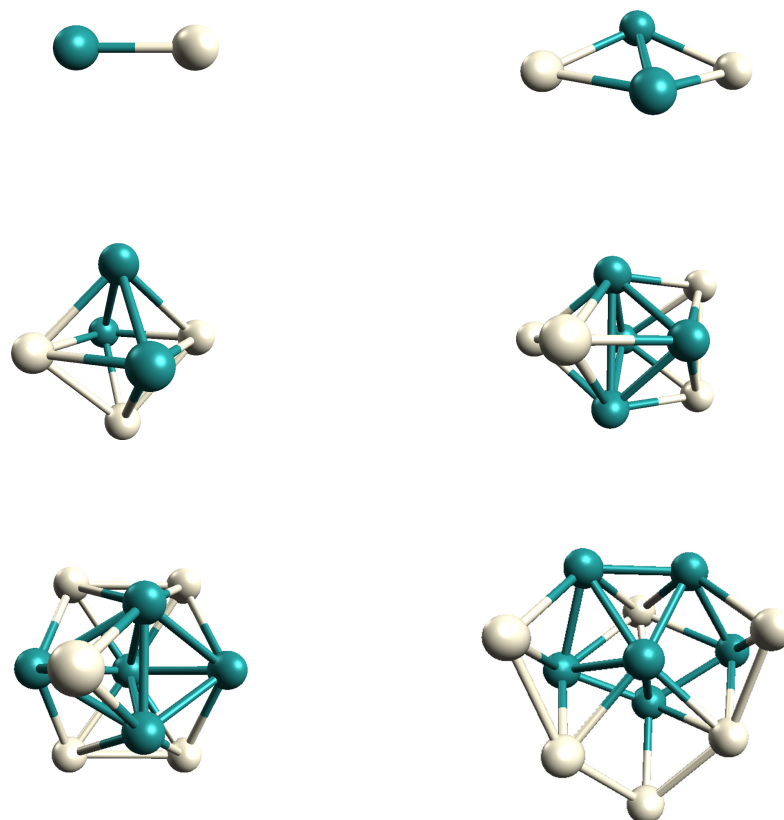


Figure 14: Ground States structures of Ru_xPt_y, X+Y ≤ 12.

References

- [1] E.W. BECKER, K. BRIER AND W. HENKES. *Z. Phys.* 146, (1956), 333 [1](#)
- [2] M. HARUTA. *Catal. Today* 36 (1997), 153 [3](#), [8](#), [9](#)
- [3] B.K. RAO, P. JENA. *Phys. Rev. B.* 32, (1985), 477
- [4] C. BINNS. *Sci. Rep.* (2001), 44, 1 [4](#)
- [5] F. BALETTO, R. FERRANDO. *Rev. Mod. Phys.* 77371, (2005) [4](#)
- [6] W.A. DE HEER. *Rev. Mod. Phys.* 65611, (1993) [4](#)
- [7] J. MEURIG, T. RICHARD, D. ADAMS, E.M. BOSWELL, B. CAPTAIN, H. GRÖNBECK, R. RAJA. *Faraday Discuss.* 138, (2008), 301 [8](#)
- [8] H. GRÖNBECK, J.M. THOMAS. *Chem. Phys. Lett.* 443, (2007), 337 [8](#)
- [9] K. SUMIYAMA, K. SUZUKI, S.A. MAKHLOUF, K. WAKOH, T. KAMIYAMA, S. YAMAMURO, T.J. KONNO, Y.F. XU, M. SAKURAI, T. HIHARA. *J. Non-Cryst. Solids.* 192, 539, (1995) [9](#)
- [10] W.P. WAGEMANS, J.H.V LENTHE, P.E.D. JONGH, A.J.V. DILLEN, K.P.D. JONG. *J. Am. Chem. Soc.* 127, 16675, (2005) [9](#)
- [11] R. AHLRICHS, S.D. ELLIOTT. *Phys. Chem. Chem. Phys.* 1, (1999), 13 [9](#)
- [12] P. HOHENBERG, W. KOHN. *Phys. Rev.* 136, 864, (1964) [13](#)
- [13] W. KOHN, L.J. SHAM. *Phys. Rev.* 140, 1133, (1965) [13](#)

REFERENCES

- [14] E. BITZEK, P. KOSKINEN, F. GAHLER, M. MOSELER, P. GUMBSCH. Phys. Rev. Lett. 97, 170201, (2006) 14, 27
- [15] B. HARTKE. J. Phys. Chem. 97, 9973, (1993) 18
- [16] D.M. DEAVEN, N. TIT, J.R. MORRIS, K.M. HO. Chem. Phys. Lett. 256, (1996), 195 18
- [17] R.L. JOHNSTON. Dalton Trans, 4193, (2003) 18
- [18] D.J. WALES, J.P.K DOYE. J. Phys. Chem. A. 101, 5111, (1997) 19, 25, 30
- [19] N. METROPOLIS, A. W. ROSENBLUTH, M. N. ROSENBLUTH, A. H. TELLER, E. TELLER. J. Chem. Phys. 21, 1087, (1953) 20
- [20] PYTHON ASE. <https://wiki.fysik.dtu.dk/ase/overview.html>. 24
- [21] SIESTA. <http://www.icmab.es/siesta/> . 25
- [22] MATERIALS STUDIO: DMOL. <http://accelrys.com/>. 25
- [23] CAMBRIDGE CLUSTER DATABASE. <http://www-wales.ch.cam.ac.uk/CCD.html>. 25
- [24] J.D. HEAD, M.C. ZERNER. Chem. Phys. Lett. 122, (1985), 264studied 27
- [25] G. ROSSI, R. FERRANDO. J. Phys. Condens. Mat. 21, 084208, (2009) 27, 36
- [26] J.P.K. DOYE, L. MEYER. Phys. Rev. Lett. 95, 063401, (2005) 32, 33
- [27] D.C. LIU, J. NOCEDAL. Mathematical Programming. Springer. (1989) 39
- [28] E. BITZEK, P. KOSKINEN. Phys. Rev. Lett. 97, 170201, (2006) 39
- [29] U. ROTH LISBERGER, W. ANDREONI. J. Chem. Phys. 94, 8129, (1991) 39, 40
- [30] B. DELLEY. J. Chem. Phys. 113, 7756, (2000) 42

REFERENCES

- [31] B. ASSADOLLAHZADEH, S. SCHAFER, P. SCHWERDTFEGER. J. Comput. Chem. 31, 8129, (2010) [44](#), [47](#), [50](#)
- [32] V.D. MORAVE, S.A. KLOPCIC, C.C. JARROLD. J. Chem. Phys. 110, 5079, (1999) [ix](#), [56](#)
- [33] F. AGUILERA-GRANJA, L.C. BALBAS, A.VEGA. J. Phys. Chem. A. 113, 13483, (2009) [57](#), [58](#), [59](#)
- [34] S. SHETTY, A.P.J. JANSEN, R.A. VAN SANTEN. THEOCHEM. 954, (2010), 109 [57](#), [59](#)